AAEC/E177

AAEC/E177
29

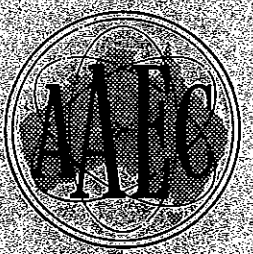

AUSTRALIAN ATOMIC ENERGY COMMISSION

RESEARCH ESTABLISHMENT
LUCAS HEIGHTS

BUCKLING AND INTEGRAL SPECTRUM MEASUREMENTS IN Pu^{239}/BeO SUB-CRITICAL ASSEMBLIES

by

P. DUERDEN

June 1967

AUSTRALIAN ATOMIC ENERGY COMMISSION

RESEARCH ESTABLISHMENT

LUCAS HEIGHTS

BUCKLING AND INTEGRAL SPECTRUM MEASUREMENTS IN Pu239/BeO SUB-CRITICAL ASSEMBLIES

by

P. DUERDEN

ABSTRACT

The materials buckling of four BeO moderated Pu239/aluminium-alloy fuelled systems having BeO/Pu239 atomic ratios of 1707, 2499, 3749 and 4999 have been measured by the exponential method. Relative fission rates of U233, U235 and Pu239 were also measured in the equilibrium spectrum region of the same assemblies. Because of the heterogeneous nature of the assemblies, fine structure corrections were applied. Some calculations using the CRAM diffusion code, and some using the GYMEA code are included.

CONTENTS

(continued)

CONTENTS (continued)

(continued)

1. INTRODUCTION

In a study of beryllium oxide moderated reactor systems, buckling and fission rate measurements have been made with Pu239/BeO systems. Similar work on U235/BeO, U235/BeO fertile material and U233/BeO assemblies has already been reported (Duerden et al. 1964; McCulloch et al. 1965; Brittliff and Duerden 1965).

2. MATERIALS

The beryllium oxide used and the measurement of its diffusion properties for thermal neutrons have been described by Brittliff et al. (1963). Slots 0.4 in. wide and 0.4 in. deep were milled along the edges of a number of the tiles so that flux scans could be made in x, y and z directions through the stacks.

The plutonium/aluminium–alloy contained 33.16 $^{w}/_{o}$ of plutonium, and was in the form of strips 25.0 in. x 1.37 in. x 0.040 in. containing 9.5 ± 0.2 g of plutonium. An isotopic analysis of the plutonium is included in Appendix 1.

Aluminium lattice plates 24 in. x 18 in. x 0.080 in. with slots 1.4 in. wide by 0.050 in. on a 2 in. pitch were available to retain the fuel plates in assemblies II, III and IV. The fuel plates were attached to 99 per cent pure aluminium plates 25 in. x 18 in. x 0.028 in. thick in Lattice I.

Details of the materials used are given in Appendix 1.

3. EXPERIMENTAL ARRANGEMENTS

The four lattices in which measurements were made had the following BeO/Pu239 atomic ratios:

Lattice I	1707
Lattice II	2499
Lattice III	3749
Lattice IV	4999

The fuel plates were always vertically orientated, that is, perpendicular to the source plane. For Lattice I the stack was approximately 18 in. x 19.4 in. x 24 in. high. 13 fuel plates, touching one another, were attached to a 25 in. x 18 in. x 0.028 in. sheet of aluminium. 17 of these fuel/aluminium layers were placed between 18 layers of BeO titles. No horizontal holes were available for flux scans in this assembly in the direction perpendicular to the fuel plates (N–S or y–direction). For Lattices II, III and IV, fuel plates were arranged in the slotted aluminium plates, which were between layers of BeO tiles. A stack 18 in. x 19.5 in. x 24 in. high was used.

The stacks were built on a graphite plinth 16 in. thick placed centrally over the IR–1 stringer hole of the Argonaut–type reactor MOATA (Marks 1962). The plinth was supported clear of the reactor shield so that a boral sheet could be slid underneath the plinth for background flux measurements.

Aluminium sheets were placed in contact with the sides of the stack and these sheets were clad with cadmium sheets. The whole assembly was then clamped together by means of a light aluminium frame. Cadmium sheets were placed horizontally on top of the BeO, in between the vertical fuel plate/aluminium sheet layers.

A general view of Stack I is given in Figure 1. Typical sections of the lattices are shown in Figures 2, 3, 4 and 5 and the positions of the measuring holes are indicated in Figure 6.

The exact composition of each lattice is listed in Appendix 1.

Aluminium scanning tubes, outside diameter 0.375 in. and wall thickness 0.022 in. were placed in the 0.4 in. x 0.4 in. channels milled in the edges of the BeO tiles. Counters were moved through these scanning tubes using remote handling equipment.

4. MEASUREMENT OF THE MATERIALS BUCKLING

Horizontal and vertical flux distributions in the stacks were measured using ¼ in. diameter BF_3 proportional counters. All counts were taken with reference to a pre-set number of pulses from a 1 in. diameter U235 fission counter fixed firmly in the reactor shield tank water at a position giving 800,000 pulses a minute at a reactor power of 5 kW. Flux scanning was thus rendered independent of drift in reactor power level. Horizontal measurements were made at 1 in. intervals to within 4 in. of the stack boundary. Vertical measurements were made at 1 in. intervals to within 4 in. of the top. The counter was frequently returned to a monitor position during the scanning period.

Pulses from the counters were fed via a head amplifier and an amplifier into a digital print-out punch-out unit. Output was thus available on paper tape and could be fed directly into the IBM 7040 computer for processing.

4.1 Relaxation Lengths

Vertical scans were made in three positions, with cadmium ratio measurements being taken. In addition, further vertical scans were made with a sheet of boral (0.25 in. thick) placed between the top of the reactor and the graphite plinth. By subtraction it was then possible to obtain the vertical flux distribution due to the required source below the stack alone, with no contribution from in-leakage of fast neutrons through the sides and top of the assembly, from the fuel plates themselves, or from γ-n neutrons produced in the BeO stack by direct gamma radiation from the reactor core.

4.1.1 Errors

The error treatment has been described by McCulloch et al. (1965). The errors considered were as follows:

	Errors (per cent.)	
	Bare	Background
(a) Counting Statistics		
Bare – not less than 1.2×10^5 per position	±0.29	
Background – not less than 0.6×10^5 per position		±0.41
(b) Control Channel Statistics		
Bare – not less than 1.2×10^6	±0.09	
Background – from 10^7 to 10^6		±0.03 to ±0.10
(c) Counter Positioning		
This was accurate to better than 1/32 inch.		
For the worst case of the shortest relaxation length this corresponds to 0.70% in flux.		
Bare – 4 positionings	±0.34	
Background – 2 positionings		±0.50
(d) Paralysis Time τ		
τ was measured as 2.6 ± 0.5 μsec. The maximum paralysis time correction was		
Bare < 0.8%	±0.16	
Background < 0.2%		±0.04

(e) Drifts in Counter Sensitivity

	Errors (per cent.) Bare	Background
The inter-channel drift was ±0.25 per cent. The resulting error contributions were		
Bare – 4 positionings	±0.13	
Background – 2 positionings		±0.18

For all lattices, combination of the above sources of error gives an overall error for the bare count of ±0.50%. The error of the background count in all cases was ±0.70%. The resulting error in the background corrected flux ranged from ±0.90% to ±0.80% as the ratio of bare count to background count varied from 2.7 to 3.0.

4.2 Extrapolated Widths

Horizontal scans were made at three different heights in the east-west direction and at two heights in the north-south direction. It was not possible to do the north-south measurements in Lattice I. Measurements were also made with the sheet of boral beneath the stack in nearly all cases. Cadmium-covered counter measurements were made as well, to ensure that only measurements in the region of the equilibrium spectrum were included in the final analysis.

4.2.1 Errors

The following sources of error were considered for bare and background horizontal flux scans.

	Errors (per cent.)
(a) Counting Statistics	
0.6×10^5 counts were taken at each position contributing	±0.41
(b) Control Channel Statistics	
Lattices I, II, III and IV – not less than 8×10^5 control counts.	±0.11
(c) Counter Positioning	
Accurate to better than 1/32 in. which corresponds to a maximum error of ±0.54 per cent. in the flux. The counter is positioned twice.	±0.38
(d) Paralysis Time	
This was measured as 2.6 ± 0.5 μsec. Maximum correction was 0.5 per cent. and within any scan the relative correction did not exceed 0.3 per cent. Resulting error is therefore	±0.04
(e) Drifts in Counter Sensitivity	
Inter-channel drift is ±0.25 per cent. The resulting error contribution for 2 positionings is	±0.18

Combination of the above errors gives a total error of less than ±0.6 per cent. in the bare or background fluxes.

The corresponding errors in the difference fluxes were less than ±0.95 per cent.

4.3 Results

Measured flux distributions are given in Appendices 2 to 6. Positional co-ordinates x, y are given in terms of distance from the east and north faces of the assembly respectively. z co-ordinates are measured from the top of the graphite plinth.

4.3.1 Cadmium ratio measurements

Boron-cadmium ratios were measured along each direction of the lattices and confirmed the existence of a constant cadmium ratio region in the lattices (Figures 7 to 10).

4.3.2 Relaxation lengths

Vertical flux distributions were fitted by the method of least squares to the function:

$$\phi = A \sinh \frac{h-z}{b_{11}} \quad ,$$

where ϕ is the flux at height z,

h is the extrapolated height,

A is an amplitude coefficient, and

b_{11} is the relaxation length.

Relaxation lengths and extrapolated heights were calculated for ranges of measurements within the constant cadmium ratio region of the lattices. The results are given in Table 1.

Examination of the table for trends in the data shows:

(i) There is no significant change of the relaxation lengths or the extrapolated height as the lower points are omitted from the range. The relaxation length and extrapolated height calculated for the largest range was therefore used in all further calculations.

(ii) There is no significant difference between the values of the relaxation length between the values of the extrapolated height calculated in the three vertical holes.

(iii) There is no significant difference between the values of the extrapolated height measured for a lattice and the weighted mean of the extrapolated heights for all the lattices. The weighted mean relaxation lengths and extrapolated heights are shown in Table 2.

4.3.3 E-W widths (x-widths)

Bare and background flux measurements were made at 1 in. intervals to within 4 in. of the stack boundaries; cadmium ratio measurements indicated that this region was of reasonably constant spectrum.

Lattices I, II and IV

No fine structure corrections were necessary for Lattices I, II, and IV.

The fluxes were least squares fitted to the function:

$$\phi = A \cos \frac{\pi}{a_x} (x - \bar{x}) \quad ,$$

both for the complete measuring range and for the range with the outermost points removed.

ϕ is the measured flux,

a_x is the extrapolated E-W width of the assembly, and $\bar{x}$ is the 'centre' of the cosine distribution.

Lattice III

Fine structure corrections had to be applied to the measured flux in Lattice III before the fluxes were least squares fitted to a cosine distribution. The correction was based

on a one-dimensional slab cell calculation and was described by Brittliff and Duerden (1965). The appropriate one-dimensional cells of the lattice are shown in Appendix 7. The maximum correction factor applied in Lattice III was 5 ±0.5 per cent. The overall error in the corrected bare flux was therefore 0.8 per cent. and in the corrected difference flux was 1.05 per cent.

The measured bare fluxes, correction factors and corrected fluxes are tabulated in Appendices 3 to 6. The results of the least squares fitting to a cosine distribution are summarised in Tables 3 and 4 for the bare and difference fluxes respectively. Examination of these tables for trends in the data shows:

(i) There is no significant change of the extrapolated width between the bare flux scans and the difference flux scans, the ratio being:

$$\frac{a_x \text{ (bare)}}{a_x \text{ (difference)}} = 1.0022 \pm 0.0013 .$$

(ii) There is no significant change of the extrapolated width as the outermost points are omitted from the distribution, the ratio being:

$$\frac{a_x \text{ (full range)}}{a_x \text{ (reduced range)}} = 1.0007 \pm 0.0015 .$$

(iii) There is no systematic trend of the extrapolated width from lattice to lattice, the mean widths being:

Lattice I $a_x = 49.87 \pm 0.16$ cm

Lattice II $a_x = 49.57 \pm 0.11$ cm

Lattice III $a_x = 51.12 \pm 0.29$ cm

Lattice IV $a_x = 50.18 \pm 0.18$ cm .

(iv) There is a systematic difference between the extrapolated widths measured at the three different heights in the stack, the ratios being:

$$\frac{a_x (z = 46.16\text{cm})}{a_x (z = 30.90\text{cm})} = 1.0128 \pm 0.0018, \quad \frac{a_x (z = 15.66\text{cm})}{a_x (z = 30.90\text{cm})} = 1.0188 \pm 0.0019 .$$

Although a third harmonic component could be present in the distribution, no least squares fitting to a third harmonic function was carried out as the results of these fittings always proved inconclusive in the previous series of experiments.

The mean fundamental width was therefore adopted for the extrapolated width measurement but with an increased error of 0.50 cm which covered the possibility that either the top or bottom mean value could be representative of the true extrapolated E-W widths of the stack.

4.3.4 N-S widths (y-widths)

Bare and background flux measurements were made at 1 in. intervals to within 4 in. of the stack boundaries. No fine structure corrections were necessary in this case. The bare and difference fluxes (when available) were fitted by least squares to the function:

$$\phi = A \cos \frac{\pi}{a_y}(y-\bar{y}) .$$

The results are summarised in Tables 5 and 6. Examination of these tables for trends in the data shows:

(i) There is no significant difference between the extrapolated widths obtained from the bare and difference flux scans, the ratio being:

$$\frac{a_y \text{ (bare)}}{a_y \text{ (difference)}} = 1.0013 \pm 0.0041 \ .$$

(ii) There is no significant difference in the extrapolated width as the outermost points are removed from the range, the ratio being:

$$\frac{a_y \text{ (full range)}}{a_y \text{ (reduced range)}} = 0.9989 \pm 0.0023 \ .$$

(iii) There is no significant systematic trend of the extrapolated width for the three lattices of similar physical width, the mean widths being:

Lattice II $a_y = 53.79 \pm 0.14$ cm

Lattice III $a_y = 53.72 \pm 0.22$ cm

Lattice IV $a_y = 53.42 \pm 0.26$ cm .

(iv) There is a significant difference between the extrapolated widths measured at the two heights in the stack, the ratio being:

$$\frac{a_y \ (z = 45.30 \text{ cm})}{a_y \ (z = 30.06 \text{ cm})} = 1.0092 \pm 0.0021 .$$

The mean bare fundamental width was adopted for the extrapolated width but with an increased error of 0.50 cm which is the same as that used for the E–W widths of the stack.

4.3.5 Stack dimensions

The overall dimensions for each stack are given in Table 7.

4.3.6 Extrapolation distances

The extrapolation distances, λ_x, λ_y, and λ_h for each of the measuring holes, as well as the appropriate mean values, are given in Table 8. They form a reasonably consistent set with a weighted mean value of 1.64 ±0.05 which is in agreement with the values found by Duerden et al. (1964).

4.3.7 The materials buckling

The buckling components calculated from the measured values of extrapolated widths and relaxation lengths for each lattice are given in Table 9. For Lattice I, an extrapolated N–S width of 53.02 ±0.23 cm was used. This is equal to the physical width plus twice the mean N–S extrapolation distance. The error used is 0.45 per cent. of the full width.

Because of the heterogeneous nature of the stacks we have:

$$K^2 = \frac{M_{\parallel}^2}{M^2}\left[\left(\frac{\pi}{a_x}\right)^2 - \left(\frac{1}{b_{11}}\right)^2\right] + \frac{M_{\perp}^2}{M^2}\left(\frac{\pi}{a_y}\right)^2 \ ,$$

where K^2 is the materials buckling of a homogeneous lattice of the same composition as the experimental stack (neglecting the effects of fine-structure flux depressions),

M^2 is the migration area in the corresponding homogeneous lattice, and

$M_{\parallel}^2$ and $M_{\perp}^2$ are the migration areas for the experimental lattice, respectively parallel and perpendicular to the slabs.

Using the method suggested by Keane (1965), one calculates $M_{\parallel}^2/M_{\perp}^2$ to be 1.008 for Lattice I and 1.024 for Lattice IV. $M_{\perp}^2$ is assumed to equal M^2. In no case does the correction to the materials buckling as calculated directly from the measured components exceed 0.3 of the experimental standard deviation.

5. INTEGRAL SPECTRUM MEASUREMENTS

Relative fission rates of U235, U233 and Pu239 using inter-calibrated fission chambers were measured as described by McCulloch et al. (1965). The counters were positioned in the centre vertical hole within the region of constant spectrum.

5.1 Flux Depression Caused by Fission Chamber Wall

The flux depression caused by the thickness of the nickel wall was measured as described by McCulloch. This flux depression was plotted as a function of spectrum hardness for each chamber, together with the values obtained by McCulloch (Figure 11). All the results were seen to be an excellent fit to a linear relation, and the least squares fitted parameters were used to obtain the depression factor for each chamber in the thermal column flux, and the depression ratio for each lattice relative to that in the thermal column.

5.2 Errors

The sources of error and their magnitudes are exactly the same as reported by Brittliff and Duerden (1965). Consideration of all these sources of error gives a total error contribution to the fission ratio per fissile atom in the range 1.73 to 1.63 per cent.

5.3 Results

The fission ratios per fissile atom are given in Table 10 whilst the measured relative count rates in the lattice are given in Appendix 8.

6. COMPARISON OF EXPERIMENTS WITH THEORY

Some calculations have been carried out using the multigroup diffusion theory code CRAM (Hassitt 1962) for a bare homogeneous spherical reactor system, and using the zero dimensional multigroup neutron diffusion code and data preparation code GYMEA (Pollard and Robinson 1966).

6.1 CRAM Calculations

The compositions used in the critical radius calculations are those of the experimental assemblies, except that for the CRAM calculations the Pu241 and Pu242 concentrations have been included with the Pu239 and Pu240 concentrations respectively.

The 18-group cross sections used for BeO, Al, Pu239 and Pu240 in the CRAM calculations are those listed by Bell et al. (1963) but were modified as follows:

BeO: Upscattering was included, based on data generated by PIXSE (McDougal 1963) using a tabulation of $S(\alpha\,\beta)$ (Sinclair 1962) obtained from LEAP (McLatchie 1962). This was included by reducing the within-the-group scattering term to maintain σ_{tr} as the value given by Bell. The values of $\sigma_{g\rightarrow g+1}$ quoted by Bell in the 18-group cross section set for groups 6-9, were found to be incorrect and were recalculated.

Pu239: The value of $\overline{\nu}$ used is that due to Smith (1964). Self-shielding was allowed for by use of the tables listed in ANL-5800.

The effective potential scattering cross section σ_p was calculated using the equivalence principle;

$$\sigma_p = \sigma_{p,f} + \frac{1}{N_a}\left[\Sigma_L + \frac{S}{4V}\right] \quad ,$$

where $\sigma_{p,f}$ is the potential scattering cross section of one isolated absorber atom present in the fuel plate,

N_a is the absorber density in the fuel plate,

Σ_L is the macroscopic scattering cross section of other atoms in the fuel plate,

S/V is the surface area to volume ratio for the fuel plate.

The self-shielding calculation for plutonium in the fuel plates gave:

Pu239 : $\sigma_p = 4.1 \times 10^3$ barns

Pu240 : $\sigma_p = 4.8 \times 10^4$ barns .

The cross sections in group 10 could be a source of error as ANL-5800 considers a group with boundaries 22.6 eV - 43 eV; Bell considers a group with boundaries 22.6 eV - 61.44 eV.

Pu240: The cross sections were obtained by modifying the 16 group cross sections listed by Bell to 18 groups. This modification kept the group 1-15 cross section set from Bell's 16-group set and included group 16-18 cross sections from Bell's 18-group set. Group 1-15 cross sections from the Bell 18-group set were not used since the size of the 1.1 eV resonance there was an order of magnitude smaller than it appears in any other set; some resonance self-shielding may be already included in these cross sections. There is a slight difference in group boundaries but this is only likely to be of importance for groups 13 and 14 as the large resonance at 1.1 eV lies on the boundary between the groups. Resonance self-shielding was calculated using curves given by Roach (1960). The cross sections used are listed in Appendix 9.

The neutron fluxes from the CRAM calculations normalised to unit total flux are listed in Appendix 10 and the normalised flux per unit lethargy unit is plotted against lethargy in Figure 12.

The materials bucklings of the assemblies were calculated using the CRAM critical radii and the experimental value of the extrapolation distance. The results together with the experimental values, are shown in Figure 14 and are listed in Table 11. The CRAM calculated value of B_m^2 is always about 5 per cent. larger than the experimental value.

Fission ratios have been obtained using the calculated neutron fluxes at the centre of the critical system (Figure 15 and Table 11). Self-shielding of the fission cross sections in the resonance region was not considered as the fissile material in the detectors is only about 2×10^{-5} cm thick. It can be seen from Figure 15 that good agreement between the calculated and experimental values of the U233/U235 ratio was obtained with the CRAM calculations but that the calculated Pu239/U235 ratios are larger than the experimental values. A similar result was found by Brittliff and Duerden (1965).

6.2 GYMEA Calculations

The compositions used in the GYMEA calculations were those of the experimental assemblies.

The neutron fluxes from the calculations, normalised to unit total flux are listed in Appendix 11 and the normalised flux per unit lethargy interval unit is included in Figure 13.

The materials bucklings are obtained directly from GYMEA and are shown in Figure 14 and listed in Table 11. Although there is good agreement with the experimental value at low BeO/Pu239 atomic density ratios, the calculated value becomes much larger than the experimental value as the BeO/Pu239 atomic density ratio in the assembly increases.

Fission ratios are obtained directly from GYMEA (Figure 15 and Table 11). The calculated Pu239/U235 ratios are similar to the experimental values but although the calculated U233/U235 ratios are in good agreement with the experimental ratios for the higher BeO/Pu239 atomic density ratio assemblies, the calculated ratios become much larger than the experimental values as the BeO/Pu239 ratio decreases.

7. CONCLUSIONS

The materials bucklings of some BeO/Pu239 lattices have been measured to an accuracy of approximately ±3 per cent. Relative fission ratios were measured to approximately ±2 per cent.

Some simple calculations were made using the computer codes CRAM and GYMEA. Similar results to those obtained by Brittliff and Duerden (1965) were found for the CRAM calculations. The calculated materials buckling was about 5 per cent. higher than the experimental value, and although good agreement between experimental and calculated values of the U233/U235 ratios was found, the calculated Pu239/U235 ratios were about 10 per cent. larger than the experimental values.

8. ACKNOWLEDGEMENTS

The author wishes to acknowledge the assistance of Miss J. Robertson in the processing of the paper tape output, and the general assistance of the MOATA Operations team.

9. REFERENCES

Argonne National Laboratory (1963). – Reactor Physics Constants. ANL–5800.

Bell, G.I., Devaney, J.J., Hansen, G.E., Mills, C.B., and Roach, W.H. (1963). – LAMS 2941.

Brittliff, E., and Duerden, P. (1965). – AAEC/E145.

Brittliff, E., Duerden, P., and McCulloch, D.B. (1963). – AAEC/TM203.

Duerden, P., McCulloch, D.B., and Brittliff, E. (1964). – AAEC/E123.

Hassitt, A. (1962). – TRG 229 (R).

Keane, A. (1965). – AAEC/TM302.

McCulloch, D.B., Duerden, P., and Brittliff, E. (1965). – AAEC/E146.

McDougal, J.D. (1963). – AEEW – M318.

McLatchie, R.F.C. (1962). – UKAEA Internal Report.

Marks, A.P. (1962). – Atomic Energy 5(4): 9–21.

Pollard, J.P., and Robinson, G.S. (1966). – AAEC/E147.

Roach, W.H. (1960). – Nucl. Sci. and Engng. 8(6): 621.

Smith, A.B. (1964). – ANL 6792.

Sinclair, R.N. (1962). – AERENP. GEN. 28.

Westcott, C.H. (1960). – AECL 1101.

APPENDIX 1

LATTICE MATERIALS

(a) Composition of Homogeneously Smeared Experimental Lattices in Atoms per cm^3

Materials	Lattice			
	I	II	III	IV
BeO	6.385×10^{22}	6.333×10^{22}	6.333×10^{22}	6.333×10^{22}
Al	3.616×10^{21}	3.877×10^{21}	3.411×10^{21}	3.178×10^{21}
Pu239	3.739×10^{19}	2.536×10^{19}	1.690×10^{19}	1.268×10^{19}
Pu240	3.204×10^{18}	2.173×10^{18}	1.449×10^{18}	1.087×10^{18}
Pu241	3.141×10^{17}	2.130×10^{17}	1.420×10^{17}	1.065×10^{17}
Pu242	1.375×10^{16}	9.322×10^{15}	6.215×10^{15}	4.661×10^{15}

(b) Mean Fuel Strip Data

External dimension of strip (in.): 25.00 x 1.366 x 0.040

Internal dimensions of Pu/Al alloy (in.): 24.05 x 1.099 x 0.020

Composition: aluminium 53.82 g

plutonium 9.475 g

Isotopic Composition of Plutonium (per cent.).

Pu239	91.329
Pu240	7.862
Pu241	0.774
Pu242	0.035

(c) Aluminium Lattice Plates

(i) Material: 99.95 per cent pure aluminium

Dimensions (in.): 24 x 18 x 0.080 (weight 860 g)

(ii) Material: 99.0 per cent pure aluminium

Dimensions (in.): 25 x 18 x 0.028 (weight 105 g)

APPENDIX 2

RELAXATION LENGTH – FLUX MEASUREMENTS

(a) Lattices I, III, IV

z (cm)	Observed Flux (arbitrary units)								
	Lattice I			Lattice III			Lattice IV		
	x=30.07 y=34.28	x=27.94 y=26.79	x=15.65 y=17.77	x=30.07 y=34.53	x=27.94 y=26.97	x=15.65 y=17.90	x=30.07 y=34.53	x=27.94 y=26.97	x=15.65 y=17.90
54.23	398.9	541.4	461.0	78.7	84.5	83.1	56.1	77.3	762.2
51.69	523.5	725.0	619.9	105.2	113.0	112.6	81.0	108.0	1011.7
49.15	665.7	905.0	781.3	133.1	145.3	140.4	104.8	137.2	1297.8
46.61	794.1	1111.7	957.5	164.1	179.5	170.3	130.4	170.0	1589.6
44.07	982.9	1314.3	1148.2	199.7	219.0	203.8	159.5	206.3	1941.0
41.53	1150.0	1533.0	1381.0	238.3	261.4	247.8	194.6	248.6	2338.1
38.99	1357.0	1837.6	1625.0	279.4	311.7	292.7	232.9	295.6	2820.5
36.45	1608.0	2105.8	1886.0	329.7	366.6	344.5	275.9	349.3	3309.8
33.91	1850.0	2434.3	2171.0	383.9	423.8	406.3	325.3	412.2	3924.5
31.37	2133.0	2870.9	2493.0	445.3	495.1	469.5	384.1	485.1	4540.8
28.83	2440.0	3219.2	2893.0	514.5	571.2	542.6	449.0	569.7	5267.5
26.29	2810.0	3769.0	3330.0	606.5	671.8	639.5	523.5	663.7	6334.7
23.75	3264.0	4348.0	3828.0	710.3	782.4	743.8	629.4	786.7	7343.6

(continued)

APPENDIX 2 (continued)

(b) Lattice II

z (cm)	Observed Flux (arbitrary units)	z (cm)	Observed Flux (arbitrary units)	
	x = 30.07 cm y = 34.53 cm		x = 27.94 cm y = 26.97 cm	x = 15.65 cm y = 17.90 cm
54.23	76.6	54.23	64.7	70.6
51.18	107.8	51.71	85.3	92.8
48.12	142.5	49.19	110.9	119.1
45.07	181.2	46.67	135.5	148.3
42.01	226.3	44.15	163.0	177.2
38.96	275.3	41.63	194.9	212.4
35.90	334.0	39.11	230.4	253.1
32.85	398.0	36.59	269.4	297.9
29.79	474.0	34.07	313.7	346.9
26.74	569.9	31.55	361.6	401.5
23.68	674.4	29.03	412.5	465.8
		26.51	480.6	535.5
		23.99	559.6	628.7

APPENDIX 3

LATTICE I. FLUX MEASUREMENTS

E – W (x) Widths

x (cm)	Observed Flux (arbitrary units)		
	z = 15.66 cm y = 31.53 cm	z = 30.90 cm y = 23.27 cm	z = 46.16 cm y = 15.02 cm
10.16	832.1	382.0	128.0
12.70	954.3	438.3	147.8
15.24	1042.4	511.1	163.4
17.78	1110.0	532.4	174.6
20.32	1159.8	532.4	181.3
22.86	1167.5	548.2	181.4
25.40	1167.8	533.9	177.2
27.94	1117.2	511.1	170.3
30.48	1039.3	476.1	160.0
33.02	942.4	426.3	146.2
35.56	803.0	366.4	126.6

APPENDIX 4

LATTICE II. FLUX MEASUREMENTS

(a) E – W (x) Widths

x (cm)	Observed Flux (arbitrary units)		
	z = 15.66 cm y = 31.76 cm	z = 30.90 cm y = 23.44 cm	z = 46.16 cm y = 15.13 cm
7.59	1132.5	686.2	218.6
10.64	1394.1	859.4	276.4
13.70	1608.4	1013.0	323.1
16.75	1772.8	1105.1	353.1
19.81	1868.6	1183.8	371.7
22.86	1896.3	1199.8	377.2
25.92	1861.7	1181.1	371.7
28.97	1751.6	1109.0	347.2
32.03	1577.1	993.4	314.6
35.08	1345.2	837.9	267.1
38.14	1051.9	655.4	209.9

(b) N – S (y) Widths

y (cm)	Observed Flux (arbitrary units)	
	z = 30.06 cm x = 35.56 cm	z = 45.30 cm x = 20.32 cm
8.33	355.5	144.9
11.63	434.2	178.5
14.93	501.1	203.7
18.23	539.7	221.7
21.53	560.9	235.7
24.83	561.5	238.5
28.13	546.5	233.5
31.43	507.4	216.5
34.73	448.1	194.3
38.03	369.2	166.8
41.33	276.8	130.9

APPENDIX 5

LATTICE III. FLUX MEASUREMENTS (ARBITRARY UNITS)

(a) E–W (x) Widths

x (cm)	z = 15.66 cm y = 31.76 cm			z = 30.90 cm y = 23.44 cm			x (cm)	z = 40.16 cm y = 15.13 cm		
	Observed Flux	Correction Factor	Corrected Flux	Observed Flux	Correction Factor	Corrected Flux		Observed Flux	Correction Factor	Corrected Flux
10.16	1511.2	1.029	1555.0	483.9	1.049	507.6	8.13	65.9	1.029	67.8
12.70	1791.2	0.962	1723.1	612.7	1.013	620.6	10.67	79.9	0.962	76.9
15.24	1964.4	0.956	1877.9	721.3	0.958	691.0	13.21	87.9	0.956	84.1
17.78	2023.3	0.962	1946.4	783.8	0.956	754.1	15.75	91.9	0.962	88.4
20.32	1988.9	1.029	2046.5	816.9	0.977	798.1	18.29	90.7	1.029	93.3
22.86	1959.2	1.050	2057.1	807.7	1.042	841.7	20.83	89.1	1.050	93.5
25.40	1994.1	1.029	2051.9	799.4	1.049	838.6	23.37	91.1	1.029	93.7
27.94	2022.3	0.962	1945.4	822.1	1.013	832.7	25.91	91.7	0.962	88.2
30.48	1905.8	0.956	1821.9	822.6	0.958	788.0	28.45	87.1	0.956	83.3
33.02	1686.6	0.962	1622.5	769.5	0.956	735.7	30.99	77.6	0.962	74.6
35.56	1367.2	1.029	1406.8	677.4	0.977	661.8	33.53	63.8	1.029	65.7

(continued)

APPENDIX 5 (continued)

LATTICE III. FLUX MEASUREMENTS

(b) N–S (y) Widths

y (cm)	Observed Flux (arbitrary units)	
	z = 30.06 cm x = 35.56 cm	z = 45.30 cm x = 20.32 cm
11.12	739.3	422.2
13.86	862.6	498.6
16.60	955.3	560.0
19.35	1019.9	609.7
22.09	1061.3	634.7
24.83	1068.5	655.1
27.57	1065.4	652.9
30.32	1030.1	626.6
33.06	978.2	586.7
35.81	880.4	536.9
38.55	770.3	476.2

APPENDIX 6

LATTICE IV. FLUX MEASUREMENTS

(a) E – W (x) Widths

x (cm)	Observed Flux (arbitrary units)		
	z = 15.66 cm y = 31.76 cm	z = 30.90 cm y = 23.44 cm	z = 46.14 cm y = 15.13 cm
10.16	1488.0	582.8	180.0
12.70	1697.7	662.3	205.2
15.24	1857.5	732.3	224.9
17.78	1984.2	782.8	241.2
20.32	2055.0	815.2	256.5
22.86	2072.9	825.9	257.4
25.40	2039.5	819.8	254.5
27.94	1971.0	781.9	249.9
30.48	1818.7	726.1	229.9
33.02	1650.3	657.1	208.4
35.56	1441.3	567.3	181.2

(b) N – S (y) Widths

y (cm)	Observed Flux (arbitrary units)	
	z = 30.06 cm x = 35.56 cm	z = 45.30 cm x = 20.32 cm
11.12	416.2	213.4
13.86	476.7	247.8
16.60	528.1	273.1
19.35	565.6	294.8
22.09	587.7	310.2
24.83	595.8	314.5
27.57	589.5	308.8
30.32	571.8	295.1
33.06	527.8	273.4
35.81	481.2	248.6
38.55	410.4	219.2

SECTION OF TOP FACE

LATTICE III

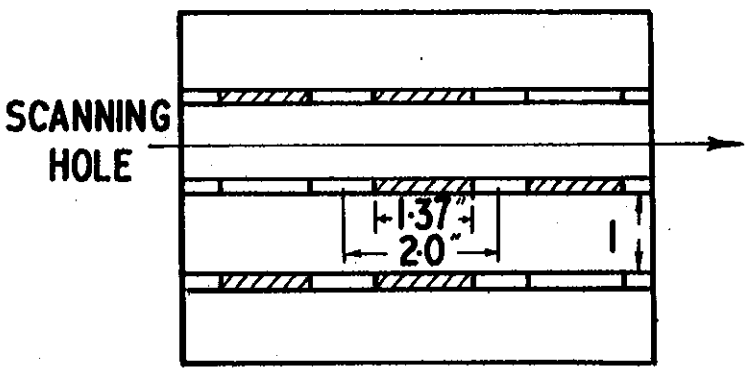

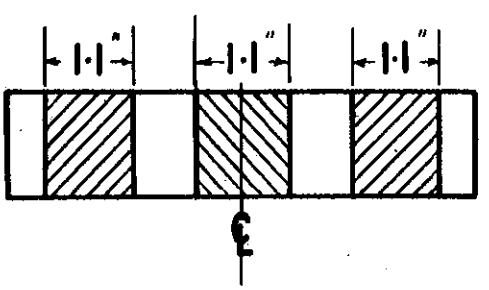

ATOMIC DENSITIES USED IN FINE STRUCTURE CALCULATIONS

BeO	$6{\cdot}338 \times 10^{22}$	throughout
AL	$3{\cdot}411 \times 10^{21}$	throughout
Pu239	$4{\cdot}648 \times 10^{19}$	in centre shaded regions
Pu239	$2{\cdot}324 \times 10^{19}$	in outer shaded regions
Pu240	$3{\cdot}968 \times 10^{18}$	in centre shaded regions
Pu240	$1{\cdot}984 \times 10^{18}$	in outer shaded regions

APPENDIX 7. CELL STRUCTURE USED FOR FINE STRUCTURE CALCULATIONS

APPENDIX 8

RELATIVE FISSION RATES IN THE LATTICES

	U235	U233	Pu239
Lattice I	1.000 ±0.009	0.499 ±0.004	0.766 ±0.006
Lattice II	1.000 ±0.009	0.445 ±0.004	0.710 ±0.006
Lattice III	1.000 ±0.009	0.395 ±0.003	0.652 ±0.006
Lattice IV	1.000 ±0.009	0.374 ±0.003	0.628 ±0.005
Thermal Column	1.000 ±0.006	0.293 ±0.002	0.471 ±0.003
*Relative Effective Number of Atoms	1.000 ±0.012	0.312 ±0.004	0.338 ±0.006

* Relative effective number of fissile atoms was calculated using effective 20.44 °C Maxwellian averaged cross sections given by Westcott (1960), namely:

σ_{f5} = 563.1 barns

σ_{f3} = 525.2 barns

σ_{f9} = 778.3 barns

APPENDIX 9

18 – GROUP CROSS SECTIONS

(a) 18 – Group Cross Sections used in CRAM Calculations

BeO

Group	σ_{tr}	σ_{rem}	$\sigma_{g\to g-3}$	$\sigma_{g\to g-2}$	$\sigma_{g\to g-1}$	$\sigma_{g\to g+1}$	$\sigma_{g\to g+2}$	$\sigma_{g\to g+3}$	$\sigma_{g\to g+4}$
1	2.172	1.324	–	–	–	1.242	0.35	0.0	0.0
2	2.455	0.732	–	–	0.0	0.700	0.12	0.0	0.0
3	5.61	2.109	–	0.0	0.0	2.109	0.0	0.0	0.0
4	6.94	1.464	0.0	0.0	0.0	1.464	0.0	0.0	0.0
5	7.65	0.971	0.0	0.0	0.0	0.971	0.0	0.0	0.0
6	8.44	0.886	0.0	0.0	0.0	0.886	0.0	0.0	0.0
7	8.83	0.982	0.0	0.0	0.0	0.982	0.0	0.0	0.0
8	9.01	0.830	0.0	0.0	0.0	0.830	0.0	0.0	0.0
9	9.06	0.835	0.0	0.0	0.0	0.835	0.0	0.0	0.0
10	9.10	1.68	0.0	0.0	0.0	1.68	0.0	0.0	0.0
11	9.10	1.6803	0.0	0.0	0.0	1.68	0.0	0.0	0.0
12	9.10	1.6804	0.0	0.0	0.0	1.68	0.0	0.0	0.0
13	9.10	1.6807	0.0	0.0	0.0	1.68	0.0	0.0	0.0
14	9.10	1.4985	0.0	0.0	0.0	1.4795	0.0171	0.0006	0.0001
15	9.10	1.1342	0.0	0.0	0.0581	1.013	0.0527	0.0085	–
16	9.10	0.604	0.0	0.0	0.1567	0.3298	0.1123	–	–
17	9.10	0.3951	0.0	0.0065	0.2869	0.0933	–	–	–
18	9.2102	0.3126	0.0014	0.1614	0.1406	–	–	–	–

Aluminium

Group	σ_{tr}	σ_{rem}	$\sigma_{g\to g+1}$	$\sigma_{g\to g+2}$	$\sigma_{g\to g+3}$
1	1.929	0.808	0.642	0.120	0.030
2	2.322	0.634	0.380	0.220	0.034
3	2.344	0.578	0.395	0.170	0.012
4	2.896	0.264	0.264	0.0	0.0
5	3.519	0.188	0.188	0.0	0.0
6	2.921	0.123	0.123	0.0	0.0
7	1.458	0.06	0.06	0.0	0.0
8	1.410	0.05	0.05	0.0	0.0
9	1.410	0.05	0.05	0.0	0.0
10	1.460	0.10	0.10	0.0	0.0
11	1.470	0.11	0.10	0.0	0.0
12	1.490	0.12	0.10	0.0	0.0
13	1.510	0.13	0.10	0.0	0.0
14	1.550	0.14	0.10	0.0	0.0
15	1.550	0.17	0.10	0.0	0.0
16	1.570	0.21	0.10	0.0	–
17	1.640	0.28	0.10	–	–
18	1.540	0.18	–	–	–

APPENDIX 9 (continued)

Pu239

Group	σ_{tr}	σ_{rem}	$\nu\sigma_f$	$\sigma_{g\to g+1}$	$\sigma_{g\to g+2}$	$\sigma_{g\to g+3}$	$\sigma_{g\to g+4}$	$\sigma_{g\to g+5}$
1	4.25	3.20	6.87	0.20	0.27	0.31	0.31	0.04
2	4.50	3.08	6.19	0.18	0.35	0.35	0.05	0.0
3	4.80	2.71	5.574	0.30	0.30	0.06	0.0	0.0
4	5.70	2.15	5.076	0.29	0.05	0.0	0.0	0.0
5	8.40	1.89	4.905	0.05	0.0	0.0	0.0	0.0
6	12.0	2.54	5.94	0.01	0.0	0.0	0.0	0.0
7	15.0	5.00	8.85	0.01	0.0	0.0	0.0	0.0
8	16.0	6.00	11.79	0.01	0.0	0.0	0.0	0.0
9	34.0	24.0	44.21	0.01	0.0	0.0	0.0	0.0
10	23.91	13.91	26.9	0.01	0.0	0.0	0.0	0.0
11	138.61	128.61	214.5	0.01	0.0	0.0	0.0	0.0
12	60.91	50.91	76.02	0.01	0.0	0.0	0.0	0.0
13	35.08	25.08	62.55	0.01	0.0	0.0	0.0	0.0
14	218.71	208.71	398.4	0.01	0.0	0.0	0.0	–
15	2155.05	2145.05	3847.6	0.01	0.0	0.0	–	–
16	647.18	637.18	1213.2	0.01	0.0	–	–	–
17	875.71	865.71	1736.0	0.01	–	–	–	–
18	937.0	927.0	1904.1	–	–	–	–	–

$\sigma_p = 4.1 \times 10^3$

Pu240

Group	σ_{tr}	σ_{rem}	$\nu\sigma_f$	$\sigma_{g\to g+1}$	$\sigma_{g\to g+2}$	$\sigma_{g\to g+3}$	$\sigma_{g\to g+4}$	$\sigma_{g\to g+5}$
1	4.25	3.22	5.952	0.24	0.33	0.55	0.40	0.05
2	4.50	2.88	5.267	0.22	0.58	0.40	0.06	0.0
3	4.65	2.41	4.587	0.50	0.35	0.06	0.0	0.0
4	5.09	1.02	2.487	0.40	0.06	0.0	0.0	0.0
5	8.20	0.33	0.159	0.05	0.0	0.0	0.0	0.0
6	11.45	0.50	0.0	0.05	0.0	0.0	0.0	0.0
7	11.70	0.75	0.0	0.05	0.0	0.0	0.0	0.0
8	13.0	2.05	0.0	0.05	0.0	0.0	0.0	0.0
9	22.0	11.05	0.0	0.05	0.0	0.0	0.0	0.0
10	65.0	54.08	0.0	0.08	0.0	0.0	0.0	0.0
11	41.0	29.09	0.0	0.09	0.0	0.0	0.0	0.0
12	39.0	24.1	0.0	0.10	0.0	0.0	0.0	0.0
13	3658.0	3153.86	4.2	3.86	0.0	0.0	0.0	0.0
14	858.0	820.35	0.6	0.35	0.0	0.0	0.0	–
15	151.0	140.07	0.0	0.07	0.0	0.0	–	–
16	251.0	240.05	0.0	0.05	0.0	–	–	–
17	341.0	330.05	0.0	0.05	–	–	–	–
18	351.0	340.0	0.0	–	–	–	–	–

$\sigma_p = 4.8 \times 10^4$

APPENDIX 9 (continued)

(b) 18-Group Fission Cross Sections Used in Fission Ratio Calculations

Group	U233	U235	Pu239
1	1.75	1.21	1.90
2	1.83	1.22	1.95
3	1.89	1.22	1.83
4	1.94	1.20	1.70
5	2.24	1.43	1.67
6	3.23	2.50	2.04
7	5.98	4.22	3.04
8	8.96	7.95	4.06
9	23.9	17.59	15.2
10	53.0	60.05	10.1
11	101.6	58.47	88.1
12	89.6	24.3	33.5
13	288.8	24.8	21.9
14	131.5	61.9	147.0
15	182.5	166.7	1576.0
16	293.2	267.4	496.8
17	457.0	473.4	608.0
18	447.0	508.7	655.0

$\sigma_p = \infty$

APPENDIX 10

ENERGY SPECTRUM AT CENTRE OF CRITICAL SPHERE (FROM CRAM)

Group	Lethargy Range (from 10 MeV)	Normalised Flux at Centre of Critical Sphere			
		Lattice I	Lattice II	Lattice III	Lattice IV
1	1.204	1100	1031	944	873
2	1.966	4465	4195	3869	3602
3	2.408	2989	2807	2571	2380
4	3.219	6032	5669	5191	4804
5	4.605	10094	9497	8710	8076
6	6.377	11420	10763	9893	9194
7	8.0	10267	9696	8935	8323
8	10.0	11703	11078	10249	9580
9	12.0	10984	10463	9747	9155
10	13.0	5279	5042	4712	4436
11	14.0	4917	4762	4503	4268
12	15.0	4696	4620	4353	4141
13	16.0	4153	4165	4051	3906
14	17.0	4171	4341	4361	4287
15	18.0	2725	3514	4337	4852
16	19.0	3155	4885	7253	9165
17	19.8	1304	2425	4267	5963
18	Thermal	545	1089	2053	2996

APPENDIX 11

NORMALISED FLUXES FROM GYMEA

Group	Lethargy Range (from 10 MeV)	Normalised Flux			
		Lattice I	Lattice II	Lattice III	Lattice IV
1	1.75	4876	4637	4300	4016
2	2.25	3889	3703	3434	3208
3	2.50	1829	1742	1615	1509
4	3.25	5621	5352	4965	4639
5	4.75	10814	10291	9562	8944
6	6.50	11272	10733	9980	9352
7	8.00	9305	8862	8253	7746
8	10.0	11813	11262	10518	9899
9	12.0	11078	10602	9953	9405
10	13.0	5191	5007	4737	4499
11	14.0	4881	4753	4533	4326
12	15.0	4549	4468	4296	4118
13	16.0	4507	4429	4264	4094
14	17.0	3988	4108	4125	4059
15	18.0	2444	3060	3655	3990
16	19.0	2290	3744	5836	7611
17	19.8	1159	2209	3950	5584
18	23.0	499	1042	2021	2993

TABLE 1

RELAXATION LENGTHS AND EXTRAPOLATED HEIGHTS

Lattice	Position		z = 49 cm → 23 cm			z = 49 cm → 26 cm			z = 49 cm →29 cm		
	x =(cm)	y =(cm)	b_{11} (cm)	h (cm)	$\Sigma \frac{\delta^2}{\sigma^2}$	b_{11} (cm)	h (cm)	$\Sigma \frac{\delta^2}{\sigma^2}$	b_{11} (cm)	h (cm)	$\Sigma \frac{\delta^2}{\sigma^2}$
I	15.65	17.77	19.40 ±0.39	62.63 ±0.59	3.3	19.58 ±0.49	62.18 ±0.62	3.0	19.82 ±0.66	61.99 ±0.66	2.7
	27.94	26.79	18.72 ± 0.30	64.49 ±0.44	13.6	18.91 ±0.38	64.22 ±0.46	12.9	19.20 ±0.51	63.87 ±0.49	12.2
	30.04	34.28	19.03 ±0.43	62.65 ±0.60	10.4	19.23 ±0.48	62.45 ±0.65	9.9	19.05 ±0.60	62.61 ±0.76	9.6

Lattice	Position		z = 51 cm → 26 cm			z = 51 cm→29 cm			z = 51 cm → 31 cm		
	x =(cm)	y =(cm)	b_{11} (cm)	h (cm)	$\Sigma \frac{\delta^2}{\sigma^2}$	b_{11} (cm)	h (cm)	$\Sigma \frac{\delta^2}{\sigma^2}$	b_{11} (cm)	h (cm)	$\Sigma \frac{\delta^2}{\sigma^2}$
II	15.65	17.90	18.21 ±0.31	61.93 ±0.33	2.8	18.05 ±0.39	62.03 ±0.37	2.4	17.95 ±0.47	62.09 ±0.40	2.4
	27.94	26.97	18.53 ± 0.37	62.17 ±0.42	1.3	18.80 ±0.52	62.00 ±0.45	0.6	18.62 ±0.67	62.10 ±0.51	0.6
	30.07	34.53	19.19 ±0.39	61.75 ±0.33	3.3	19.42 ±0.51	61.64 ±0.36	2.7	18.85 ±0.54	61.93 ±0.38	2.7
III	15.65	17.90	17.08 ±0.25	64.13 ±0.52	7.2	17.10 ±0.33	64.11 ±0.59	7.2	16.67 ±0.37	64.64 ±0.68	4.9
	27.94	26.97	18.05 ±0.30	61.92 ±0.33	2.9	18.31 ±0.39	61.75 ±0.36	1.7	18.13 ±0.47	61.86 ± 0.38	1.5
	30.07	34.53	18.00 ±0.24	62.64 ±0.21	2.9	18.23 ±0.31	62.54 ±0.22	1.1	18.17 ±0.48	62.53 ±0.44	1.0
IV	15.65	17.90	16.68 ±0.24	62.63 ±0.40	9.3	16.99 ±0.31	62.34 ±0.40	6.5	16.60 ± 0.35	62.67 ±0.47	4.7
	27.94	26.97	16.57 ±0.24	62.93 ±0.42	0.3	16.50 ±0.30	63.01 ±0.48	0.2	16.53 ±0.37	62.97 ± 0.50	0.1
	30.07	34.53	16.55 ±0.24	61.73 ±0.33	2.2	16.41 ±0.28	61.85 ±0.37	1.6	16.27 ±0.35	61.95 ±0.41	1.3

TABLE 2

MEAN RELAXATION LENGTHS AND EXTRAPOLATED HEIGHTS

Lattice	b_{11} (cm)	h (cm)
I	19.09 ±0.14	63.26 ±0.23
II	18.57 ±0.19	61.95 ±0.22
III	17.68 ±0.15	62.59 ±0.17
IV	16.60 ±0.14	62.32 ±0.22

Weighted Mean of Extrapolated Heights 62.52 ±0.12 cm.

TABLE 3

EXTRAPOLATED x–WIDTHS (BARE)

Lattice	Position		a_x (cm)	$\Sigma \frac{\delta^2}{\sigma^2}$	a_x (cm)	$\Sigma \frac{\delta^2}{\sigma^2}$
	z = (cm)	y = (cm)	10.16 cm < x < 35.56 cm		12.70 cm < x < 33.02 cm	
I	15.66	31.53	49.86 ±0.23	20.6	50.08 ±0.44	12.8
	30.90	23.27	49.35 ±0.29	9.9	49.34 ±0.53	9.4
	46.16	15.02	50.40 ±0.30	14.5	50.98 ±0.56	9.9
	Position		7.59 cm < x < 38.14 cm		10.64 cm < x < 35.08 cm	
II	15.66	31.76	50.11 ±0.22	4.4	50.18 ±0.35	0.5
	30.90	23.44	49.01 ±0.17	6.0	48.83 ±0.32	4.8
	46.16	15.15	49.58 ±0.17	5.9	50.04 ±0.35	2.8
	Position		10.16 cm < x < 35.56 cm		12.70 cm < x < 33.02 cm	
III	15.66	31.76	51.75 ±0.52	11.1	51.18 ±0.94	7.2
	30.90	23.44	50.40 ±0.48	4.1	50.77 ±0.91	3.9
	46.16	15.13	51.22 ±0.52	5.1	50.57 ±0.89	4.4
IV	15.66	31.76	50.69 ±0.31	2.5	50.40 ±0.55	1.9
	30.90	23.44	49.76 ±0.29	4.5	49.27 ±0.53	1.7
	46.16	15.13	50.09 ±0.32	21.6	49.53 ±0.56	14.8

TABLE 4

EXTRAPOLATED x–WIDTHS (DIFFERENCE)

Lattice	Position		a_x (cm)	$\Sigma \frac{\delta^2}{\sigma^2}$	a_x (cm)	$\Sigma \frac{\delta^2}{\sigma^2}$
	z = (cm)	y = (cm)	10.16 cm < x < 35.56 cm		12.70 cm < x < 33.02 cm	
I	15.66	31.53	49.67 ±0.35	17.0	50.13 ±0.70	11.0
	30.90	23.27	49.67 ±0.44	7.0	49.85 ±0.85	6.9
	46.16	15.02	50.62 ±0.49	11.3	51.30 ±0.92	8.5
	Position		7.59 cm < x < 38.14 cm		10.64 cm < x < 35.06 cm	
II	15.66	31.76	49.90 ±0.25	3.3	49.61 ±0.55	0.5
	30.90	23.44	48.84 ±0.25	3.6	48.61 ±0.51	2.8
	46.16	15.13	49.27 ±0.25	3.8	49.84 ±0.54	1.8
	Position		10.16 cm < x < 35.56 cm		12.70 cm < x < 33.02 cm	
III	15.66	31.76	51.83 ±0.57	8.5	51.54 ±1.04	6.0
	30.90	23.44	49.91 ±0.51 *	3.5	49.79 ±0.95 *	3.0
	46.16	15.13	51.11 ±0.54	3.5	50.53 ±0.97	3.1
IV	15.66	31.76	50.93 ±0.51	6.8	51.24 ±0.95	6.6
	30.90	23.44	49.86 ±0.46	2.0	49.58 ±0.85	1.4
	46.16	15.13	50.14 ±0.51 x	18.7	48.66 ±0.85	11.6

* Data at position x = 13.86 cm contributes a $\left(\frac{\delta}{\sigma}\right)^2 > 9$ which exceeds our rejection criterion.

x Data at position x = 15.24 cm contributes a $\left(\frac{\delta}{\sigma}\right)^2 > 9$ which exceeds our rejection criterion.

These points have been rejected before calculating the above fittings.

TABLE 5

EXTRAPOLATED y–WIDTHS (BARE)

Lattice	Position		a_y (cm)	$\Sigma \frac{\delta^2}{\sigma^2}$	a_y (cm)	$\Sigma \frac{\delta^2}{\sigma^2}$
	z = (cm)	x = (cm)	8.33 cm < y < 41.33 cm		11.63 cm < y < 38.03 cm	
II	30.06	35.56	53.08 ±0.18	6.3	53.40 ±0.36	4.8
	45.30	20.32	54.50 ±0.20	7.3	54.52 ±0.38	7.3
	Position		11.12 cm < y < 38.55 cm		13.86 cm < y < 35.81 cm	
III	30.06	35.56	54.42 ±0.32	4.2	55.43 ±0.62	2.3
	45.30	20.32	53.01 ±0.30	3.7	52.48 ±0.55	1.8
IV	30.06	35.56	53.52 ±0.37	7.5	53.88 ±0.70	2.6
	45.30	20.32	53.31 ±0.35	14.4	52.29 ±0.61	6.2

TABLE 6

EXTRAPOLATED y–WIDTHS (DIFFERENCE)

Lattice	Position		a_y (cm)	$\Sigma \frac{\delta^2}{\sigma^2}$	a_y (cm)	$\Sigma \frac{\delta^2}{\sigma^2}$
	z = (cm)	x = (cm)	11.12 cm < y < 38.55 cm		13.86 cm < y < 35.81 cm	
III	30.06	35.56	54.22 ±0.50	3.2	55.05 ±0.96	2.3
	45.30	20.32	53.05 ±0.47	2.1	52.24 ±0.80	1.4

TABLE 7

MEASURED STACK DIMENSIONS (cm)

Lattice	E–W Width $(a_x)_{Phys}$	N–S Width $(a_y)_{Phys}$	Height $(h)_{Phys}$
I	46.43 ±0.10	49.81 ±0.15	61.05 ±0.05
II	46.43 ±0.10	50.17 ±0.15	61.05 ±0.05
III	46.43 ±0.10	50.17 ±0.15	61.05 ±0.05
IV	46.43 ±0.10	50.17 ±0.15	61.05 ±0.05

TABLE 8

EXTRAPOLATION DISTANCES (cm)

Lattice		I	II	III	IV
E–W 15 cm level	λ_x	1.72 ±0.25	1.85 ±0.24	2.67 ±0.53	2.14 ±0.33
E–W 31 cm level	λ_x	1.47 ±0.31	1.30 ±0.19	1.99 ±0.50	1.68 ±0.31
E–W 46 cm level	λ_x	1.99 ±0.32	1.58 ±0.19	2.40 ±0.54	1.84 ±0.34
N–S 30 cm level	λ_y	–	1.46 ±0.23	2.13 ±0.35	1.68 ±0.40
N–S 45 cm level	λ_y	–	2.16 ±0.25	1.43 ±0.33	1.58 ±0.38
Vertical North	λ_h	1.58 ±0.59	0.88 ±0.33	3.08 ±0.52	1.58 ±0.40
Vertical Centre	λ_h	3.44 ±0.41	1.12 ±0.42	0.87 ±0.33	1.88 ±0.42
Vertical South	λ_h	1.60 ±0.60	0.70 ±0.33	1.59 ±0.21	0.68 ±0.33

Mean E–W	λ_x	1.71 ±0.08
Mean N–S	λ_y	1.75 ±0.12
Mean Vertical	λ_h	1.44 ±0.12

Mean extrapolated distance = 1.66 ±0.06 cms.

TABLE 9

MATERIALS BUCKLING

Lattice	$\left(\frac{\pi}{a_x}\right)^2$ (m^{-2})	$\left(\frac{\pi}{a_y}\right)^2$ (m^{-2})	$\left(\frac{1}{b_{11}}\right)^2$ (m^{-2})	K^2 (m^{-2})
I	39.65 ±0.40	35.11 ± 0.35	27.44 ±0.60	47.4 ±0.8
II	39.65 ±0.40	34.27 ±0.35	29.00 ±0.59	45.1 ±0.8
III	39.65 ±0.40	34.27 ±0.35	31.99 ±0.54	42.1 ±0.7
IV	39.65 ±0.40	34.27 ±0.35	36.29 ±0.61	37.7 ±0.8

TABLE 10

MEASURED FISSION RATIOS

Lattice	Fission Ratio Per Fissile Atom	
	Pu239/U235	U233/U235
I	2.261 ±0.038	1.596 ±0.027
II	2.094 ±0.036	1.422 ±0.024
III	1.918 ±0.033	1.258 ±0.021
IV	1.845 ±0.031	1.192 ±0.020

TABLE 11

COMPARISON OF EXPERIMENTAL RESULTS AND CALCULATIONS

MATERIALS BUCKLINGS (m^{-2})

Lattice	Experimental	Calculated (CRAM)	Calculated (GYMEA)
I	47.4 ±0.8	48.53	46.32
II	45.1 ±0.8	46.72	45.66
III	42.1 ±0.7	43.69	44.42
IV	37.7 ±0.8	40.79	42.27

FISSION RATIOS

Lattice	Pu239/U235			U233/U235		
	Experimental	Calculated (CRAM)	Calculated (GYMEA)	Experimental	Calculated (CRAM)	Calculated (GYMEA)
I	2.261 ±0.038	2.368	2.309	1.596 ±0.027	1.563	1.794
II	2.094 ±0.036	2.347	2.195	1.422 ±0.024	1.411	1.509
III	1.918 ±0.033	2.252	2.033	1.258 ±0.021	1.280	1.292
IV	1.845 ±0.031	2.169	1.924	1.192 ±0.020	1.212	1.188

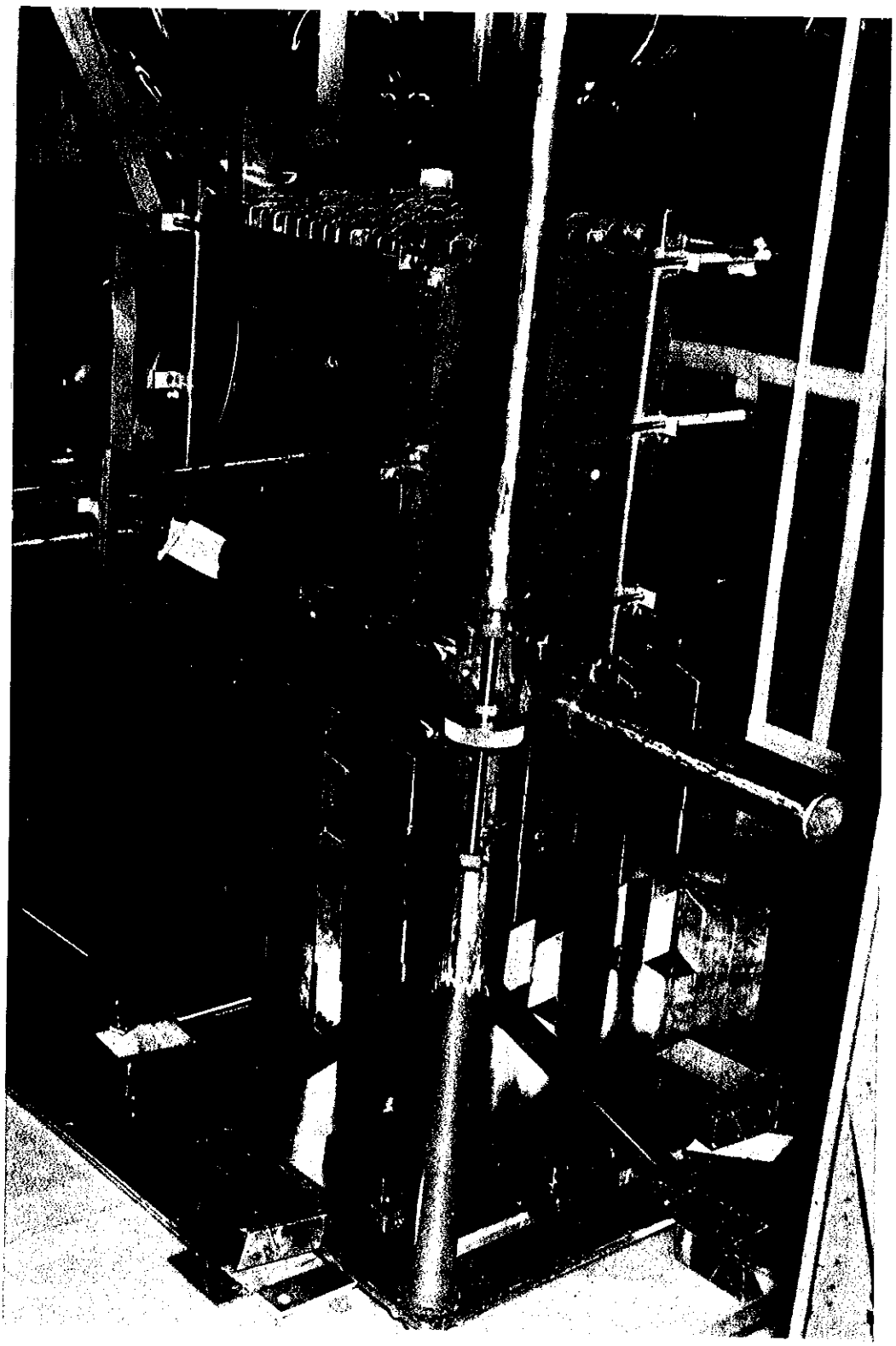

FIGURE 1. GENERAL VIEW OF SUB-CRITICAL ASSEMBLY

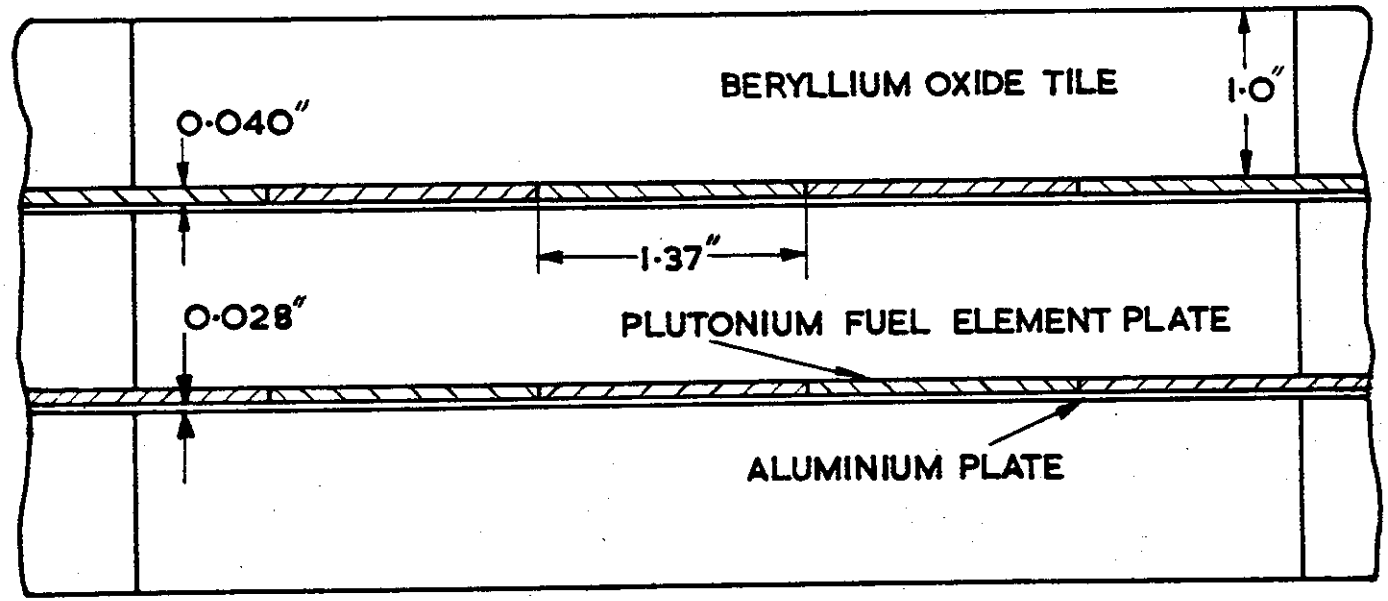

FIGURE 2. LATTICE I REPRESENTATIVE SECTION OF TOP FACE

P954

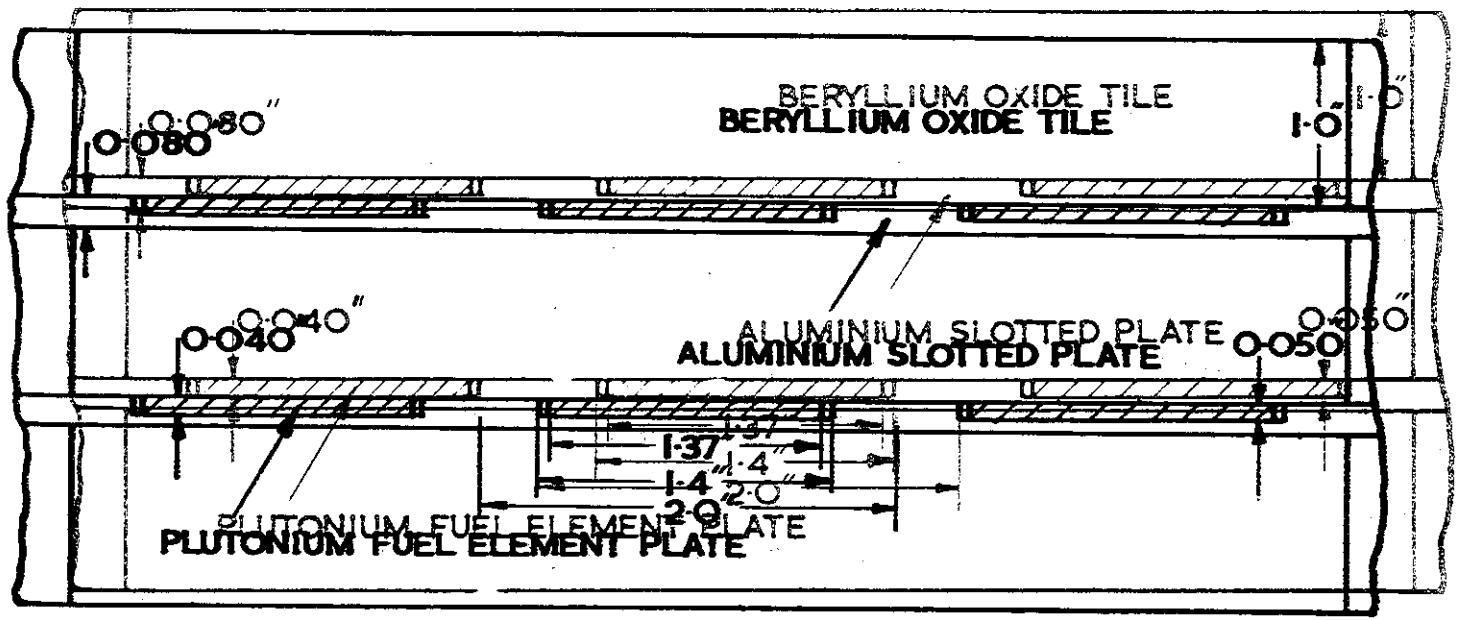

FIGURE 3. LATTICE II REPRESENTATIVE SECTION OF TOP FACE

FIGURE 3. LATTICE II REPRESENTATIVE SECTION OF TOP FACE

 P954

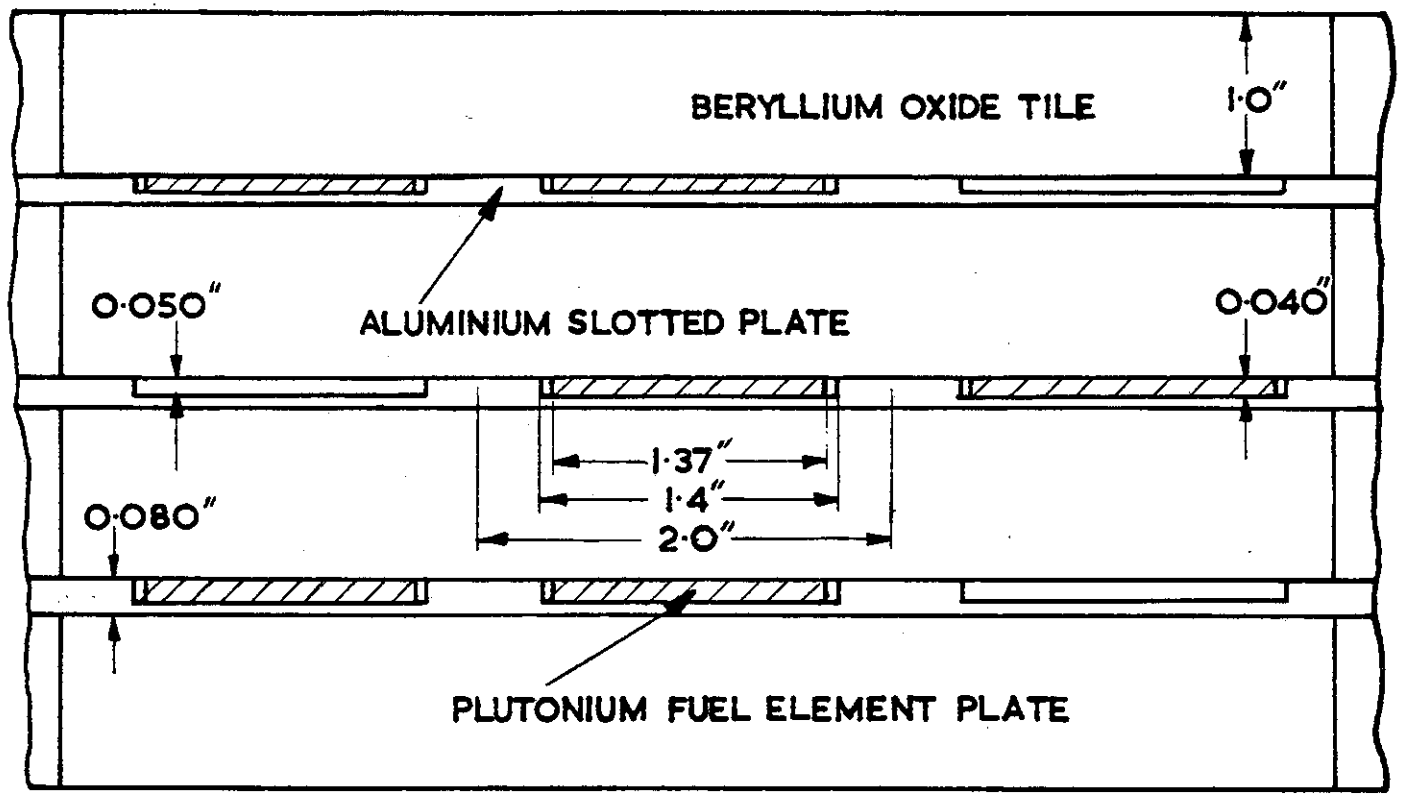

FIGURE 4. LATTICE III REPRESENTATIVE SECTION OF TOP FACE

P954

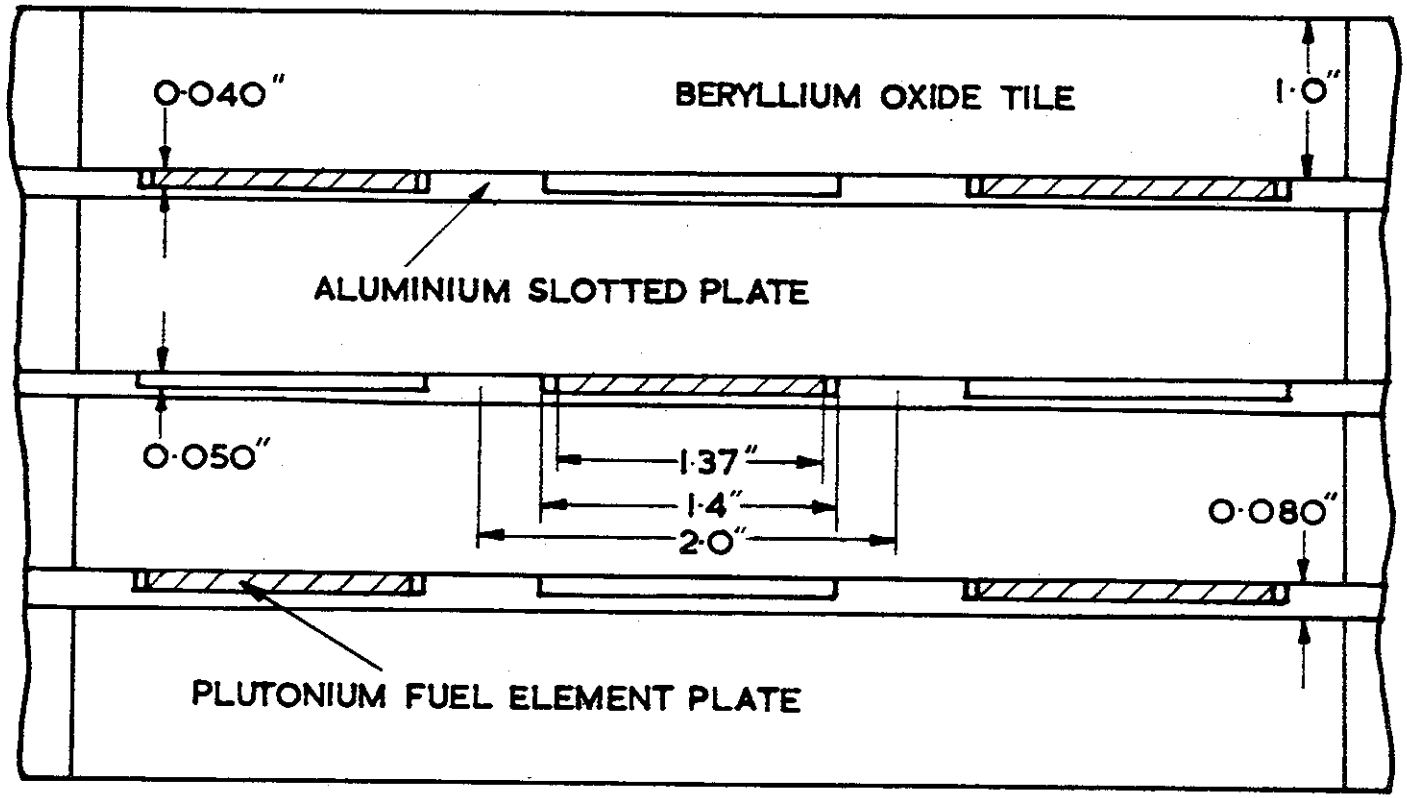

FIGURE 5. LATTICE IV REPRESENTATIVE SECTION OF TOP FACE

P954

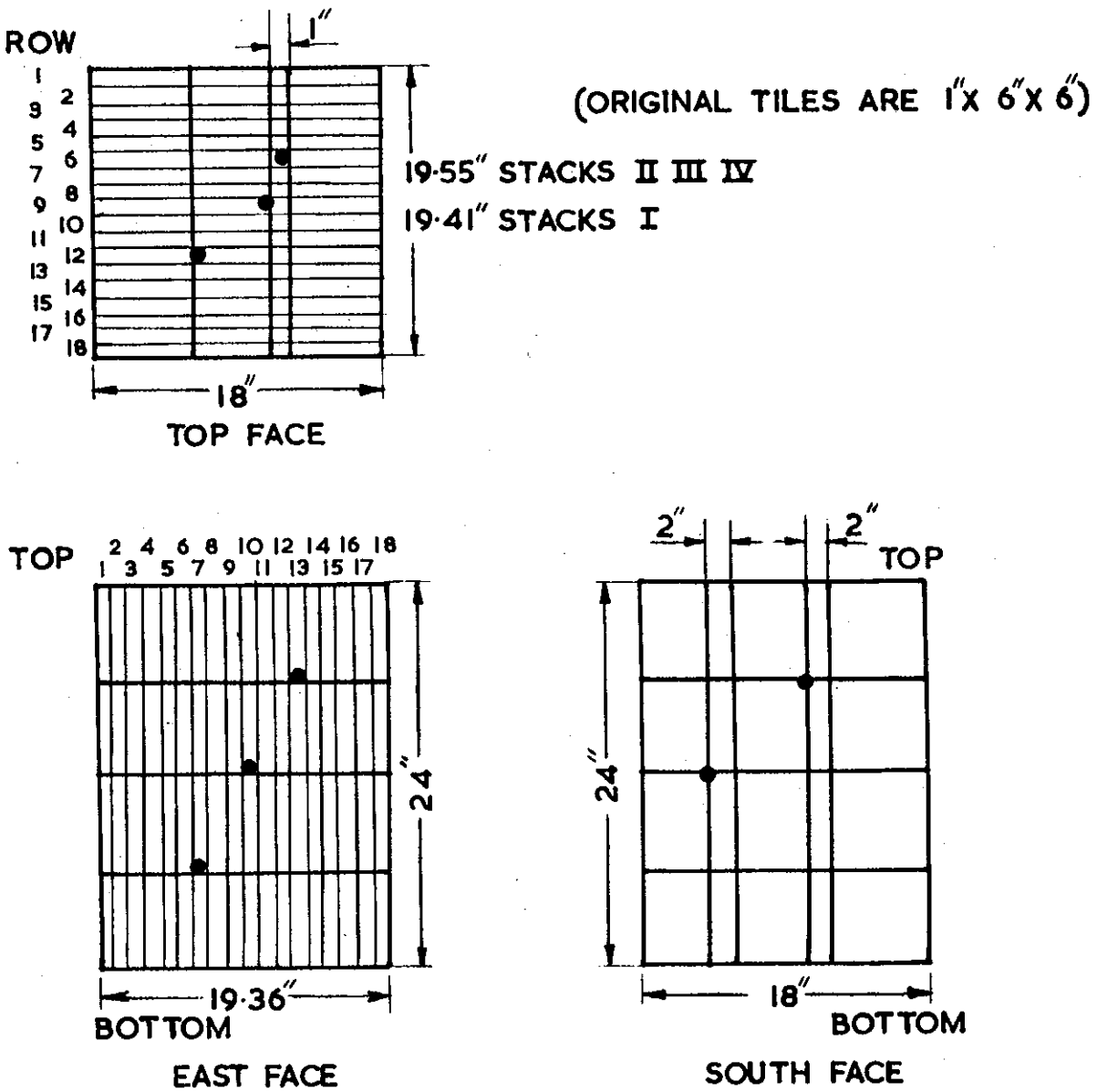

FIGURE 6. SCANNING HOLE POSITIONS IN LATTICES I,II III AND IV

P954

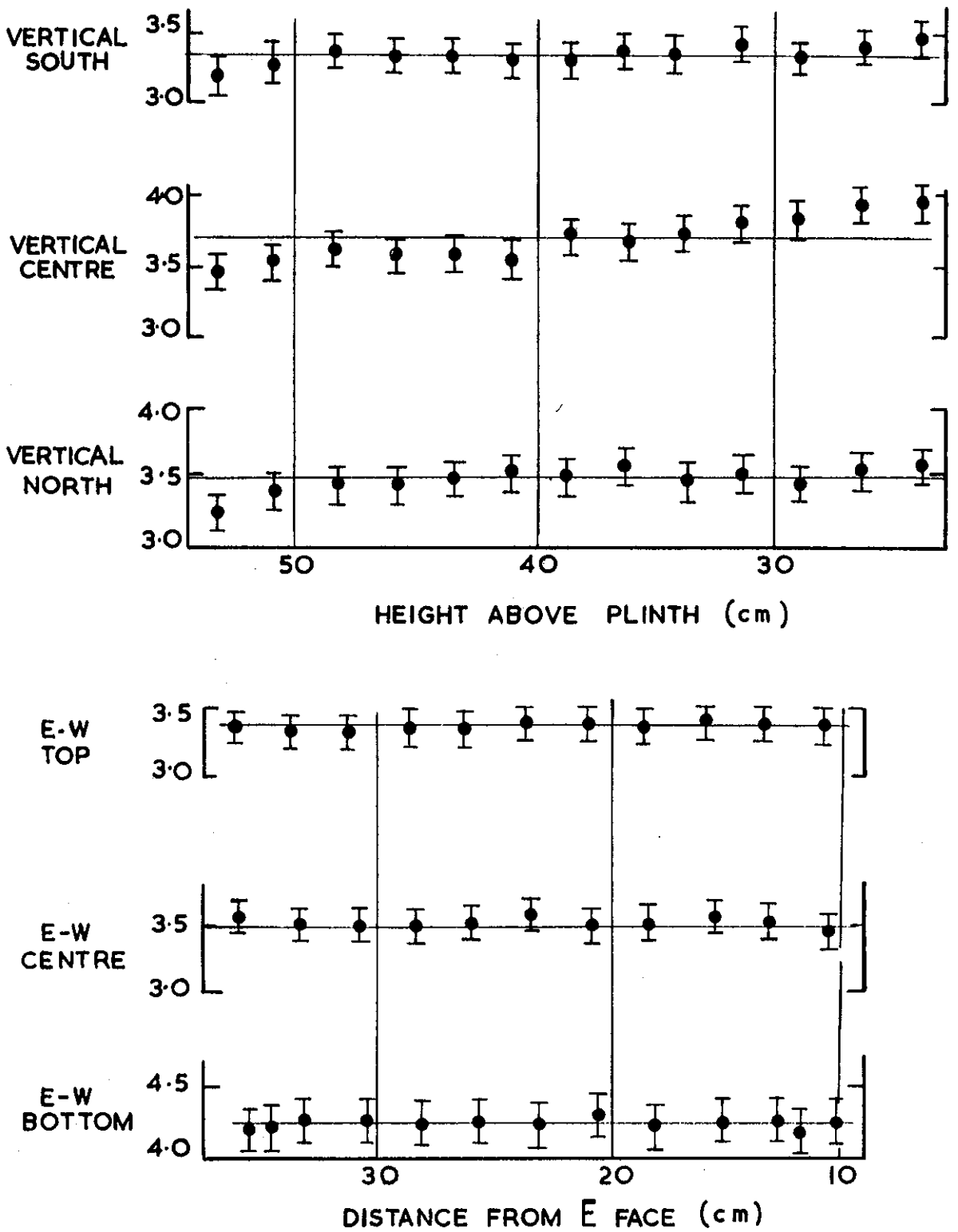

FIGURE 7. CADMIUM RATIOS FROM FLUX SCANS IN LATTICE I

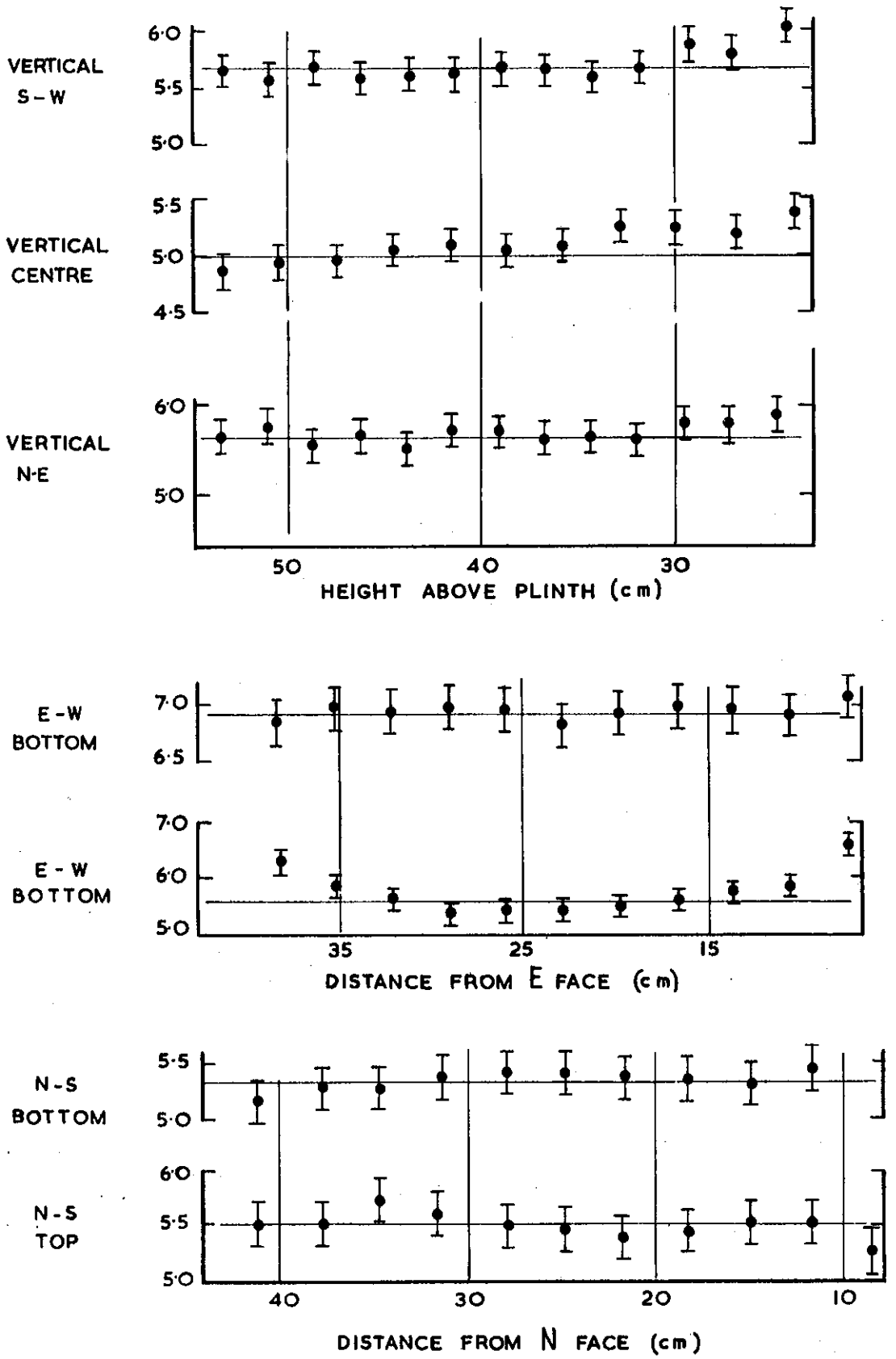

FIGURE 8. CADMIUM RATIOS FROM FLUX SCANS IN LATTICE II

P954

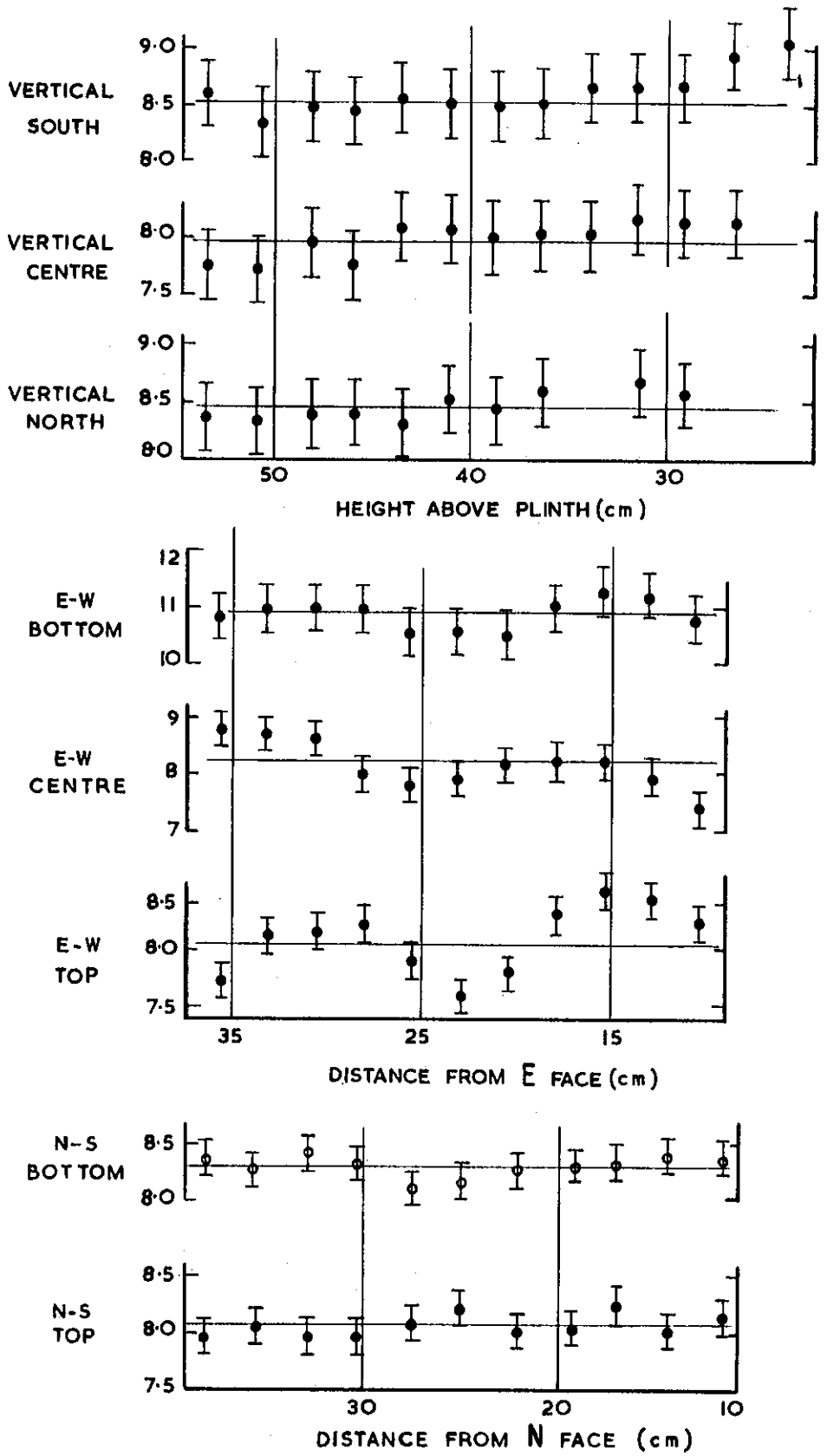

FIGURE 9. CADMIUM RATIOS FROM FLUX SCANS IN LATTICE III

P954

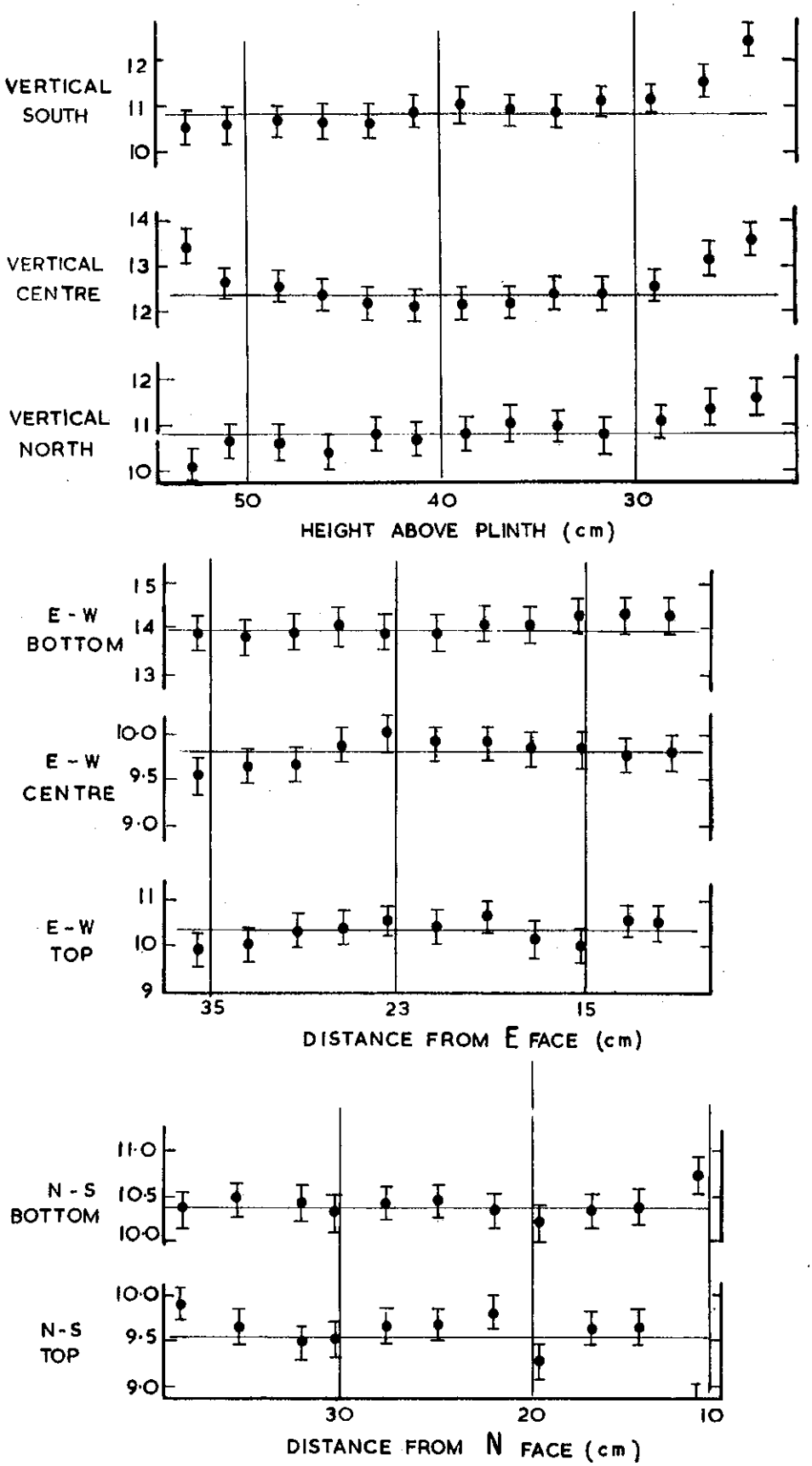

FIGURE 10. CADMIUM RATIOS FROM FLUX SCANS IN LATTICE IV

P954

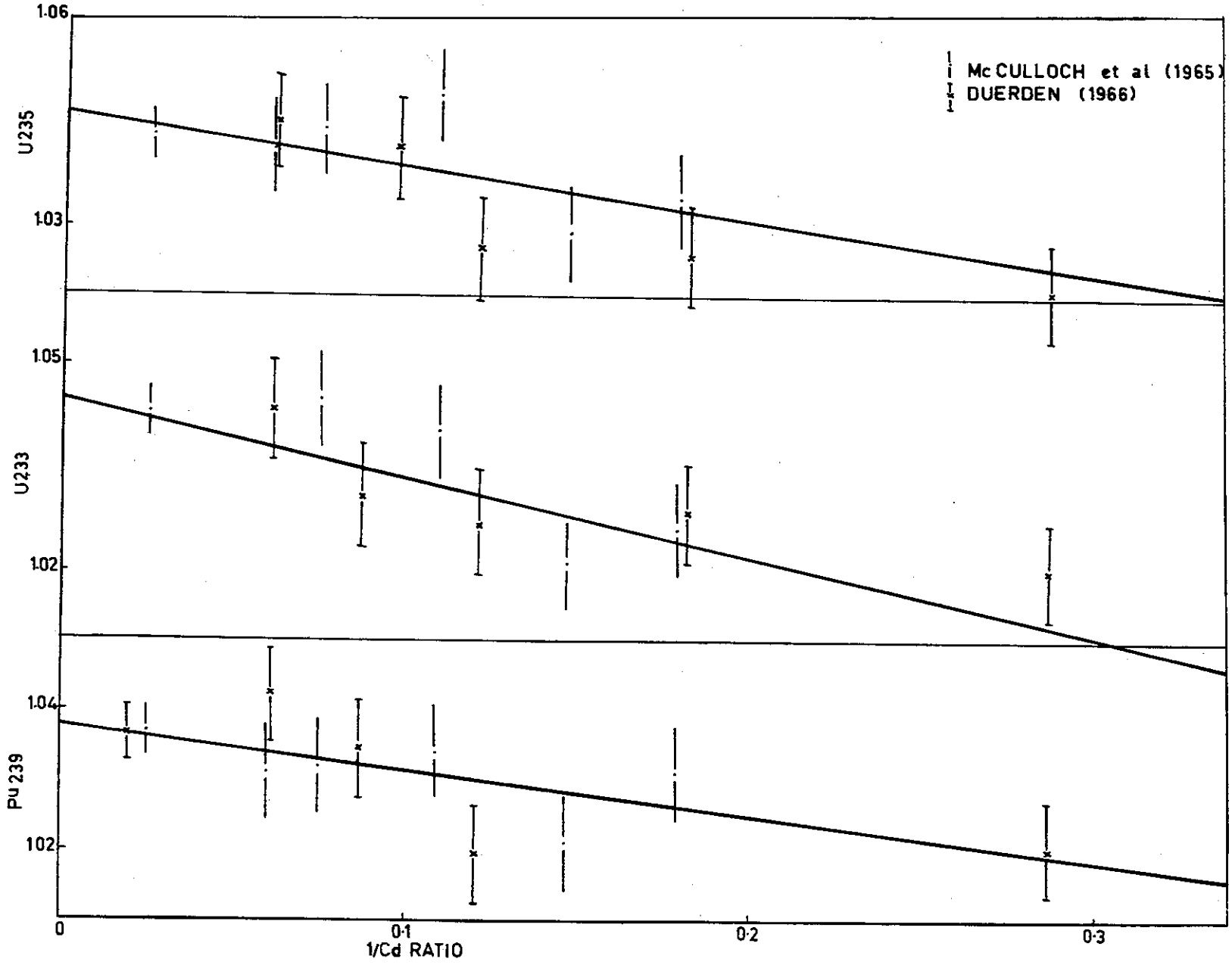

FIGURE 11. FLUX DEPRESSIONS BY NICKEL WALLS

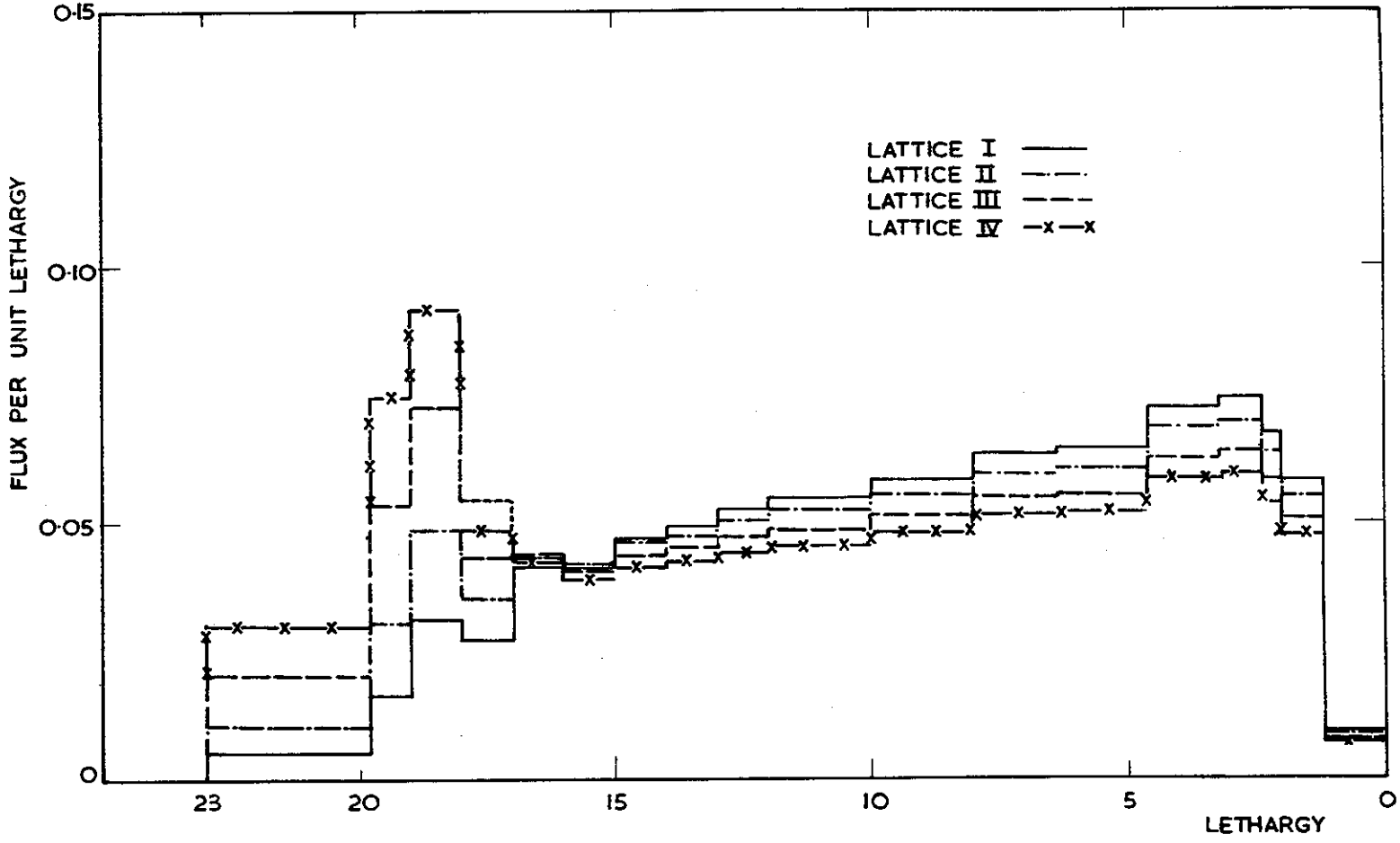

FIGURE 12. NORMALISED FLUX PER UNIT LETHARGY INTERVAL FROM CRAM CALCULATIONS

P954

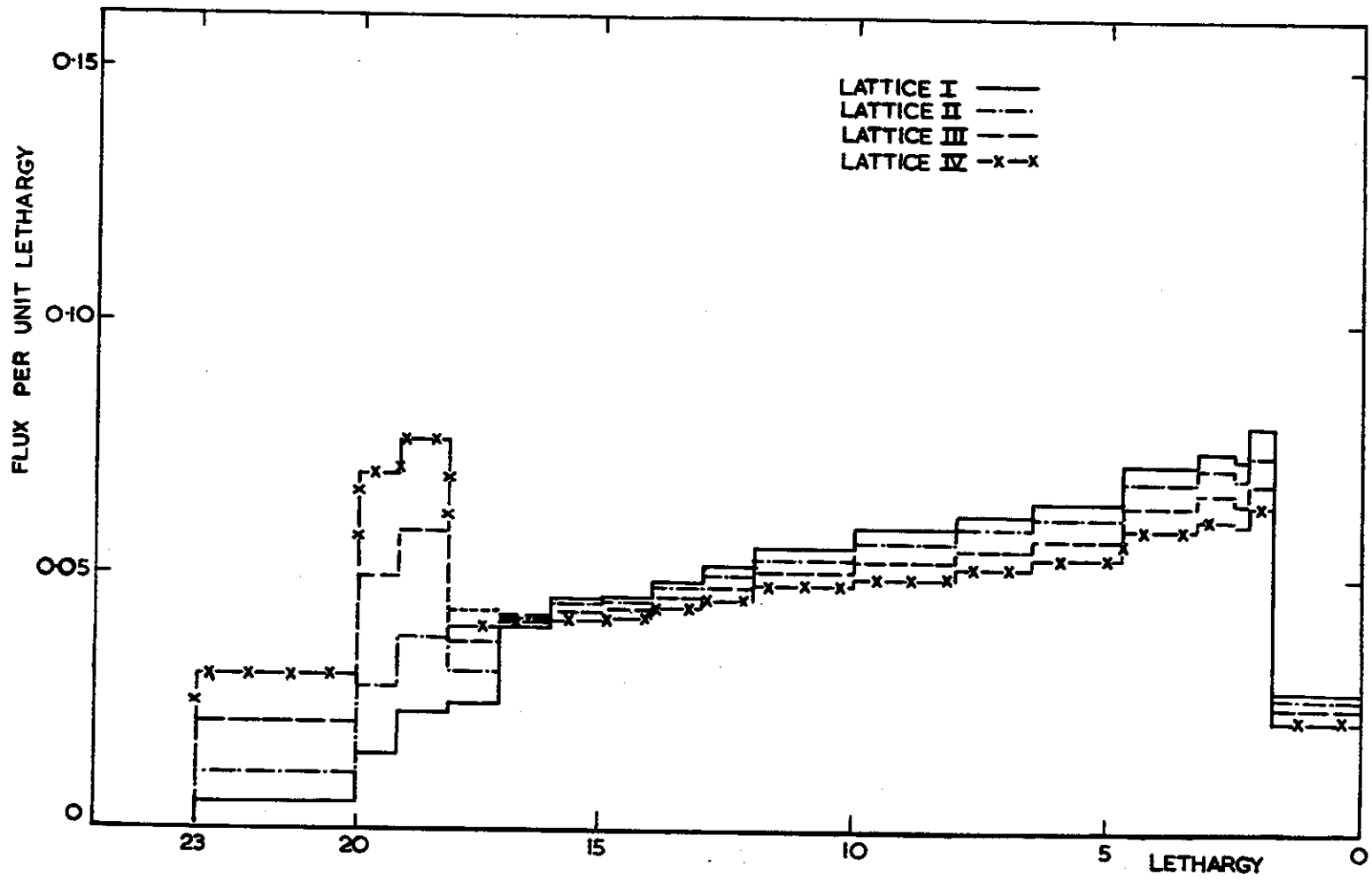

FIGURE 13. NORMALISED FLUX PER UNIT LETHARGY INTEGRAL FROM GYMEA CALCULATIONS

P954

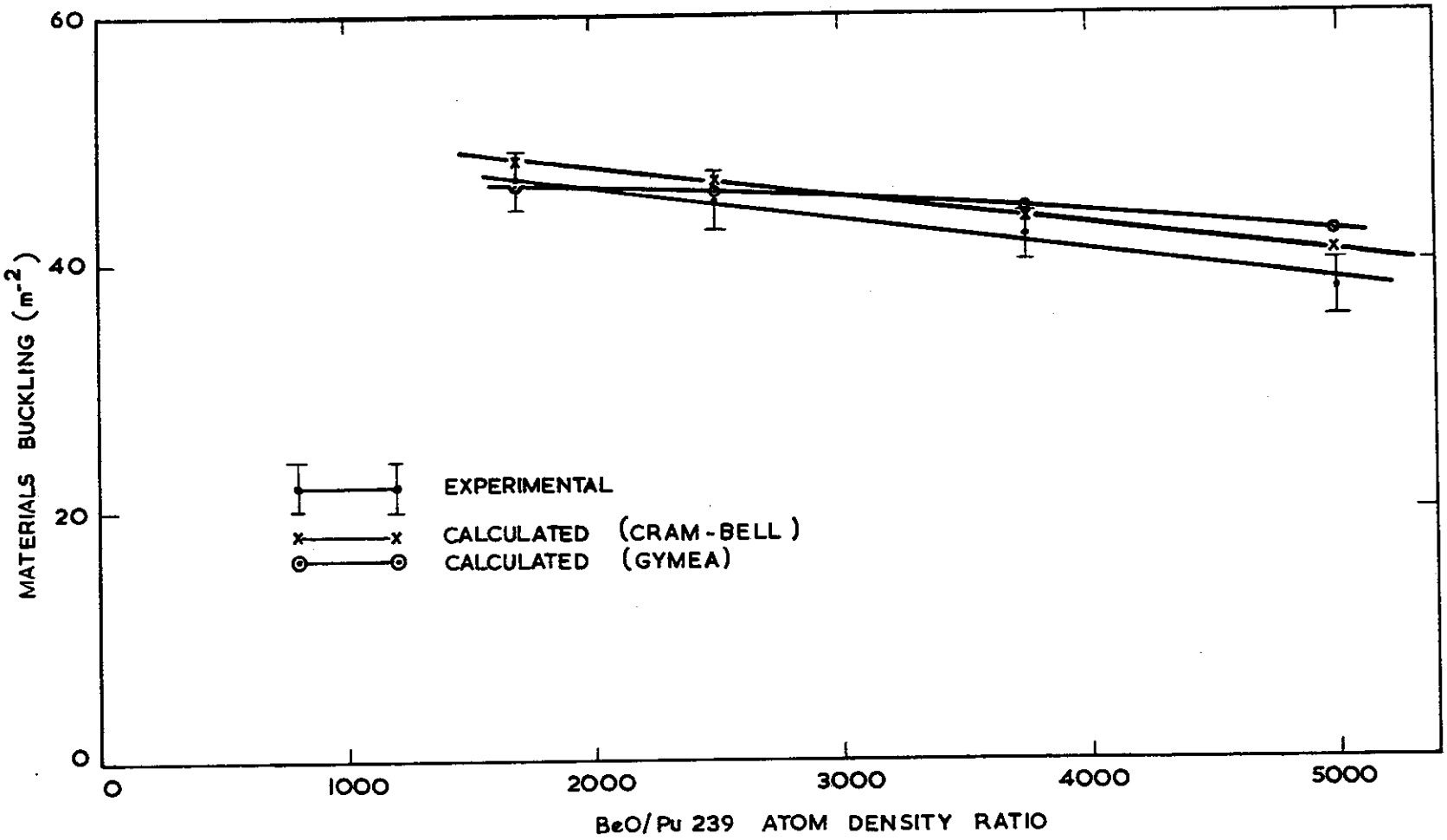

FIGURE 14. CALCULATED AND EXPERIMENTAL MATERIALS BUCKLING

P954

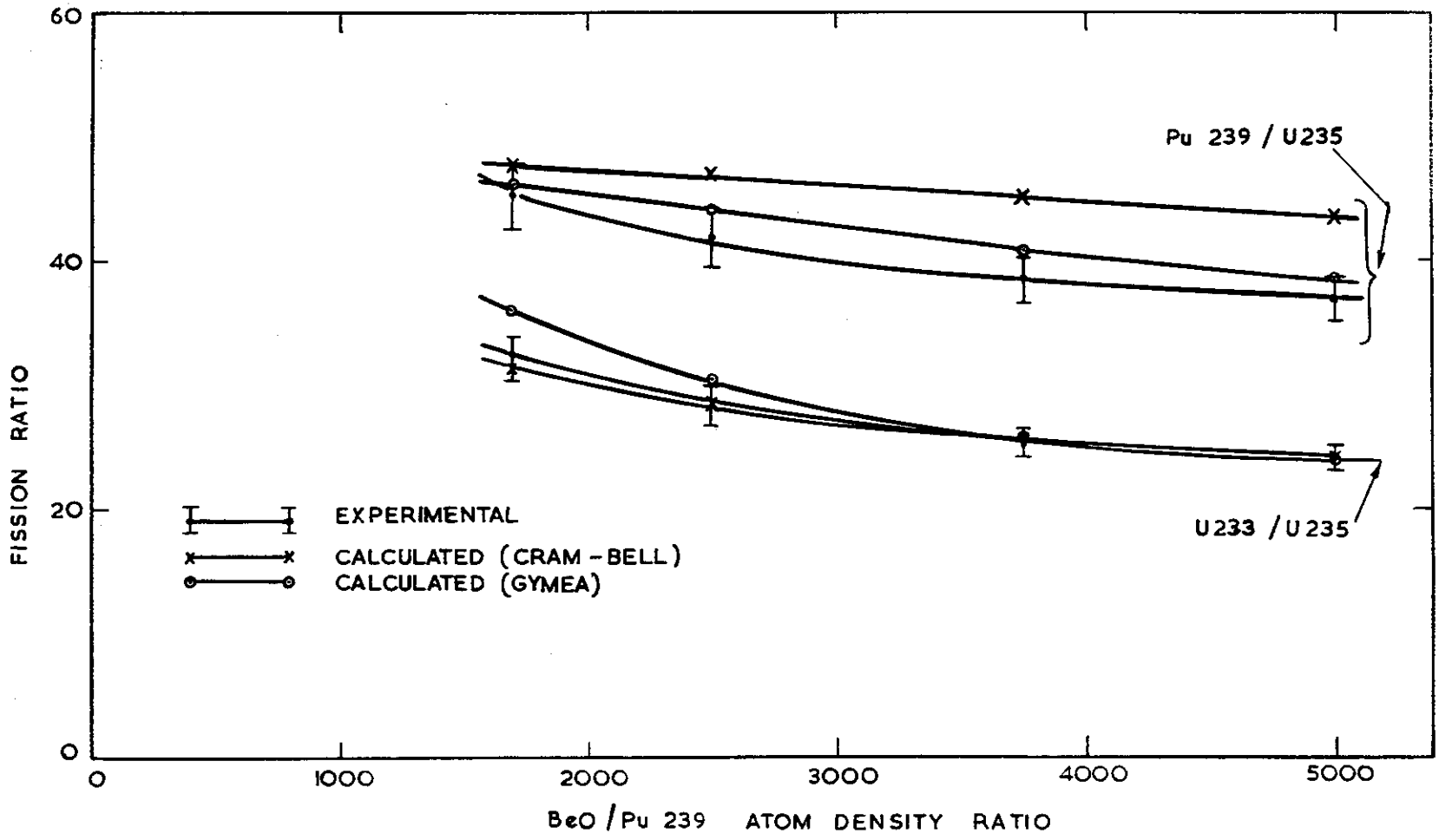

FIGURE 15. CALCULATED AND EXPERIMENTAL FISSION RATIOS

P954